UC Davis
UC Davis Previously Published Works

Title

Active Basalt Alteration at Supercritical Conditions in a Seawater-Recharged Hydrothermal System: IDDP-2 Drill Hole, Reykjanes, Iceland

Permalink

https://escholarship.org/uc/item/9w73w765

Journal

Geochemistry Geophysics Geosystems, 22(11)

ISSN

1525-2027

Authors

Zierenberg, Robert A
Friðleifsson, Guðmundur Ó
Elders, Wilfred A
et al.

Publication Date

2021-11-01

DOI

10.1029/2021gc009747

Peer reviewed

Active Basalt Alteration at Supercritical Conditions in a Seawater-Recharged Hydrothermal System: IDDP-2 Drill Hole, Reykjanes, Iceland

Robert A. Zierenberg[1] , Guðmundur Ó. Friðleifsson[2], Wilfred A. Elders[3], Peter Schiffman[1], and Andrew P. G. Fowler[4]

[1]Department of Earth and Planetary Sciences, University of California, Davis, Davis, CA, USA, [2]IDDP, Gardabaer, Iceland, [3]Department of Earth and Planetary Sciences, University of California, Riverside, CA, USA, [4]Department of Earth and Environmental Sciences, University of Minnesota, Minneapolis, MN, USA

Abstract The 4.5 km deep IDDP-2 drill hole was drilled at Reykjanes, Iceland, in an active seawater-recharged hydrothermal system on the landward extension the Mid-Atlantic Ridge. Drilling targeted a well-defined hydrothermal up-flow zone feeding the Reykjanes geothermal reservoir, which produces fluids compositionally equivalent to basalt-hosted deep sea hydrothermal vents. Spot cores recovered from depths between 3,648 to 4,659 m depths consist of pervasively altered sheeted diabase dikes. The shallowest core has an alteration mineral assemblage similar to the producing geothermal reservoir but is being overprinted by the underlying Hornblende Zone assemblage dominated by labradorite and hornblende. The deepest cored section (4,634–4,659 m) retains a diabasic texture, but all primary minerals are replaced or have changed composition. Plagioclase ranges from An_{30} to An_{99} and igneous augite is replaced by intergrown hornblende, clinopyroxene, and orthopyroxene. Hydrothermal biotite and potassium feldspar formed locally due to reaction with a phase-separated brine, indicated by co-existing vapor-rich and salt + vapor-rich fluid inclusions. Seawater-derived supercritical hydrothermal fluid entering the bottom of the bore hole actively phase separates due pressure drop controlled by the fluid levels in the drill hole. Felsic veins, present in trace amounts, record a continuous transition from magmatic to hydrothermal conditions, including incipient hydrous melting. The vertical changes observed in mineralogy and mineral chemistry indicate that fluids from the deep high temperature reaction zone can undergo significant cooling and reaction with host rocks along their path to the seafloor.

Plain Language Summary Many important geologic processes including plate tectonics are driven by the transfer of heat from the deep Earth to the near surface. Volcanic rocks that erupt beneath the oceans at seafloor spreading centers are a fundamental aspect of such transfer of heat energy. Circulation of seawater through mid-ocean ridge spreading centers changes the composition of both the volcanic rocks and the seawater and makes a fundamental contribution to the chemical and energy balance of the Earth. On the Reykjanes Peninsula, a landward extension of the Mid-Atlantic Ridge, the Iceland Deep Drilling Project recovered drill core from the seawater-recharged Reykjanes geothermal field down to ~4.5 km depth, where pressure-temperature conditions are identical to those inferred to control the composition of submarine hot springs on the mid-ocean ridges. The volcanic rocks are pervasively altered forming new minerals, but primary rock texture remains well preserved. The chemical exchange in the deep rocks occurs at approximately 800°C, well above the temperature expected where cracks form in the rocks that allow fluids to circulate. The present day in situ temperature at 4.5 km depth ~550°–600°C and fluids produced from that depth could potentially become a low carbon source to generate geothermal electricity.

1. Introduction

The goal of the Iceland Deep Drilling Program (IDDP) is to investigate the feasibility of producing electric power from supercritical geothermal fluids whose chemical properties are shaped by reaction with the host rocks (Friðleifsson et al., 2014). The IDDP-2 penetrated a geochemical analog for basalt-hosted sea-floor hydrothermal systems that produce black smokers. Seawater-rock interaction at mid-ocean ridges is the dominant source of thermal and chemical exchange between the lithosphere and the hydrosphere, yet

direct observation of the products of these reactions has been inaccessible until now. The IDDP-2 drill hole provided the first core samples recovered from the high temperature reaction zone (HTRZ) of an active seawater-recharged hydrothermal system at supercritical conditions. Although the amount of core recovered from this system is small, detailed studies of this core, reported here, illustrate the importance and utility of cores in studies of active hydrothermal system.

In this paper, we focus on the hydrothermal alteration observed in drill core recovered from seven different depth intervals spanning 3,648–4,659 m down hole (Friðleifsson, Albertsson, et al., 2020; Friðleifsson, Elders, et al., 2020; Friðleifsson, Pálsson, et al., 2020) (Figure 1). Note, downhole depths differ from true vertical depths owing to the inclination of the drill hole from vertical; all depths quoted in this report are total down hole lengths unless expressly referred to as "vertical depth." The bottom part of the hole was angled to intercept the hydrothermal up flow zone that feeds the Reykjanes geothermal field (Figure 2), which supplies steam to produce 100 MWe of electric power. These cores record the transition from the presently exploited geothermal reservoir at Reykjanes, which extends down to near 3,000 m, into the high temperature reaction zone at ~4,500 m vertical depth. The deepest cores record evolved seawater-rock alteration in a sheeted dike complex at temperatures well above supercritical conditions for seawater. The altered basaltic rocks at 4.5 km depth are presently at temperatures near the brittle-ductile transition (~600–650°C; Violay et al., 2012, 2015). These observations have important implications for understanding the processes that control the composition of hydrothermal fluids venting at mid-ocean ridges. Additional documentation of observations and data in support of this paper can be found in Supporting Information S1, which can be accessed using the link provided in Acknowledgments and Data Availability Statement.

1.1. Geologic Setting

The Reykjanes geothermal system is situated in the neovolcanic zone of Iceland's Southwest Rift Zone, the on-land extension of the slow spreading (1.8 cm/yr; Sigmundsson et al., 2020) Mid Atlantic Ridge. Tholeiitic basalt flows from fissure-fed eruptions cover most of the Reykjanes Peninsula and surround low-lying linear ridges of basalt hyaloclastite formed from subglacial fissure eruptions during previous glacial stages (Figure 2) (Franzson et al., 2002; Jakobsson et al., 1978; Saemundsson et al., 2020). At the time this paper was submitted, the most recent lavas were tholeiitic basalts from the Reykjanes Fires, which erupted in the early 13 century and include the Stampar lavas that mostly cover the western half of the Reykjanes promontory. Subsequently, on March 19, 2021, primitive basalt began erupting from fissures northeast of Grindavik, in Geldingadalir, located the Reykjavik and Krýsuvik spreading segments (Figure 2). Less abundant "picritic" lavas make up the Háleyjabunga lava shield east of Reykjanes geothermal field. Gee et al. (1998) characterized the "picritic" lavas as trace element-depleted (TED) based on low incompatible element abundances and Nb/Zr ratios <0.07. Most of the lavas and hyaloclastites exposed on the Reykjanes Peninsula are classified as trace element-enriched (TEE) by Gee et al. (1998) and are compositionally similar to mid-ocean ridge basalts. The geologic history of the Reykjanes geothermal field, including the distribution of subsurface alteration mineralogy and present-day temperature structure, is well constrained by more than 36 drill holes that explore the active geothermal system (Friðleifsson, Elders, et al., 2020). Subaerial lavas from the upper 20–50 m of the stratigraphy are underlain by subglacial and submarine basalt, hyaloclastite and marine sediment down to approximately 1.5 km depth, where intrusive basalt, mainly dikes, become increasingly dominant with depth (Figure 1). Sheeted dikes are present at depths below ~2.5 km, including both TEE and TED related dikes (Fowler & Zierenberg, 2016; Friðleifsson et al., 2017). Whereas the volcanic rock composition, structure and stratigraphy are similar to typical oceanic crust formed at slow spreading ridges, excess melting from the Iceland Hot Spot results in increased crustal thickness that reaches approximately 16 km thick at Reykjanes (Allen et al., 2002), compared to normal oceanic crust that is ~7 km thick (White et al., 1992). Hydrothermal alteration increases from zeolite grade to amphibolite grade with depth (Fowler & Zierenberg, 2016; Fowler et al., 2015; Lonker et al., 1993; Marks, Schiffman, Zierenberg, Elders, et al., 2010; Marks et al., 2011; Tómasson & Kristmannsdóttir, 1972). Prograde mineral assemblages are comparable to those attributed to seafloor metamorphism in ophiolites (Evarts & Schiffman, 1983; Spooner & Fyfe, 1973) and oceanic crust (Alt et al., 1996, 2010; Humphris & Thompson, 1978).

The surface of the Reykjanes geothermal field (Figure 2) is mostly 20–40 m above sea level and is only a few kilometers from the ocean which surrounds it on three sides. Below a shallow (20–60 m) perched
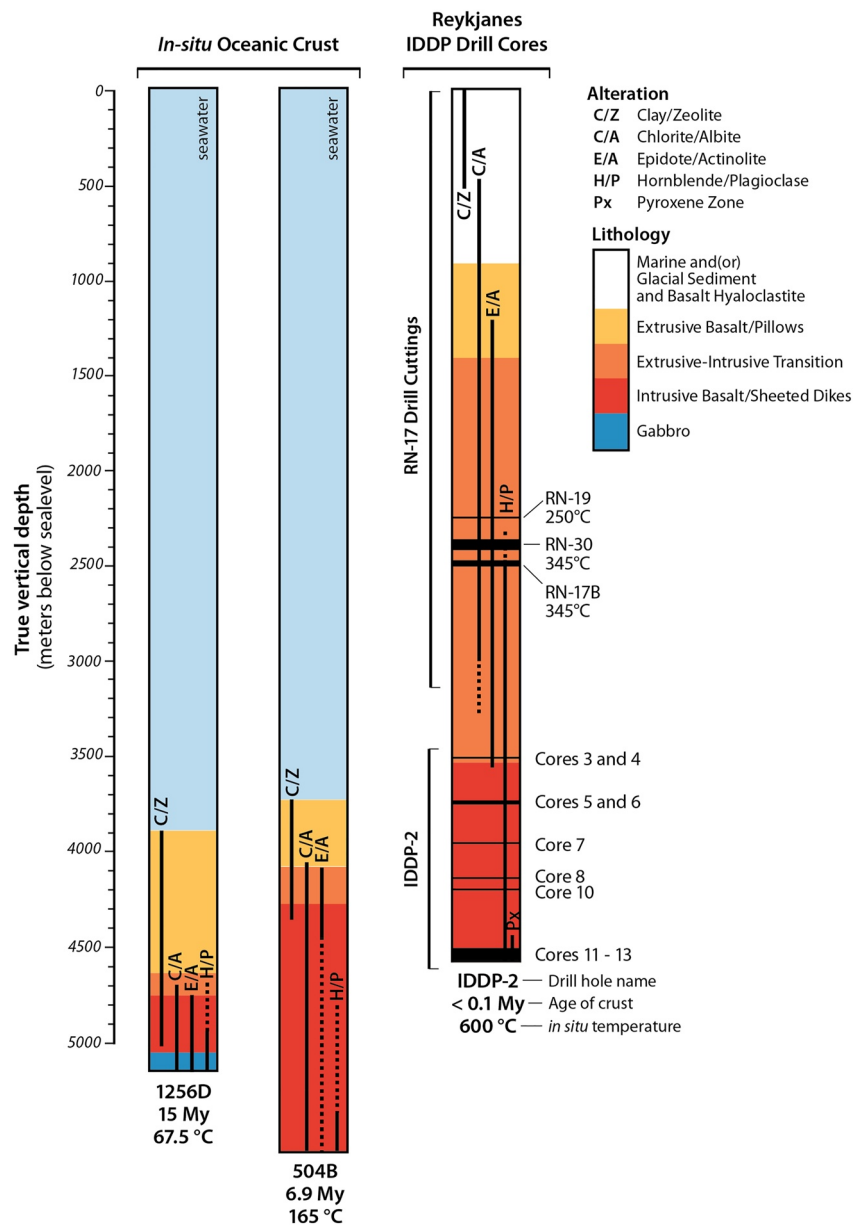
Figure 1. Comparison of the lithology, alteration, age, and temperature of the Reykjanes Geothermal Field with sections of the oceanic crust as determined by recovery of drill core elsewhere. The righthand column summarizes data from IDDP-2 well, the subject of this paper, and observations made in other Reykjanes geothermal wells. Data from scientific drill holes 504B and 1256D are from Alt et al. (1996, 2010) and contained references.

fresh-water lens, the porous basaltic rocks are saturated with seawater (Sigurdsson, 1986). The geothermal fluid produced for electric generation at Reykjanes has seawater salinity and is compositionally indistinguishable from submarine geothermal, "black smoker," fluids for most conservative elements (Figure 3) (Ármannsson, 2016; Arnórsson et al., 1978; Ólafsson & Riley, 1978; Pope et al., 2009). Reykjanes fluids are somewhat enriched in boron (Figure 3e) and alkali elements (normalized to chloride), similar to the Endeavor Ridge geothermal fluids (Figure 3f), which are proposed to have a small component of sediment-derived constituents (Butterfield et al., 1994; Lilley et al., 2003; Paduan et al., 2018). However, the Reykjanes fluids do not show elevated levels of methane or ammonia (Óskarsson, Fridriksson, & Thorbjörnsson, 2015; Óskarsson, Inguaggiato, et al., 2015), nor do they show time variability in salinity due to active near seafloor phase separation (Butterfield et al., 1994). Not only is the Reykjanes geothermal fluid characteristic of black
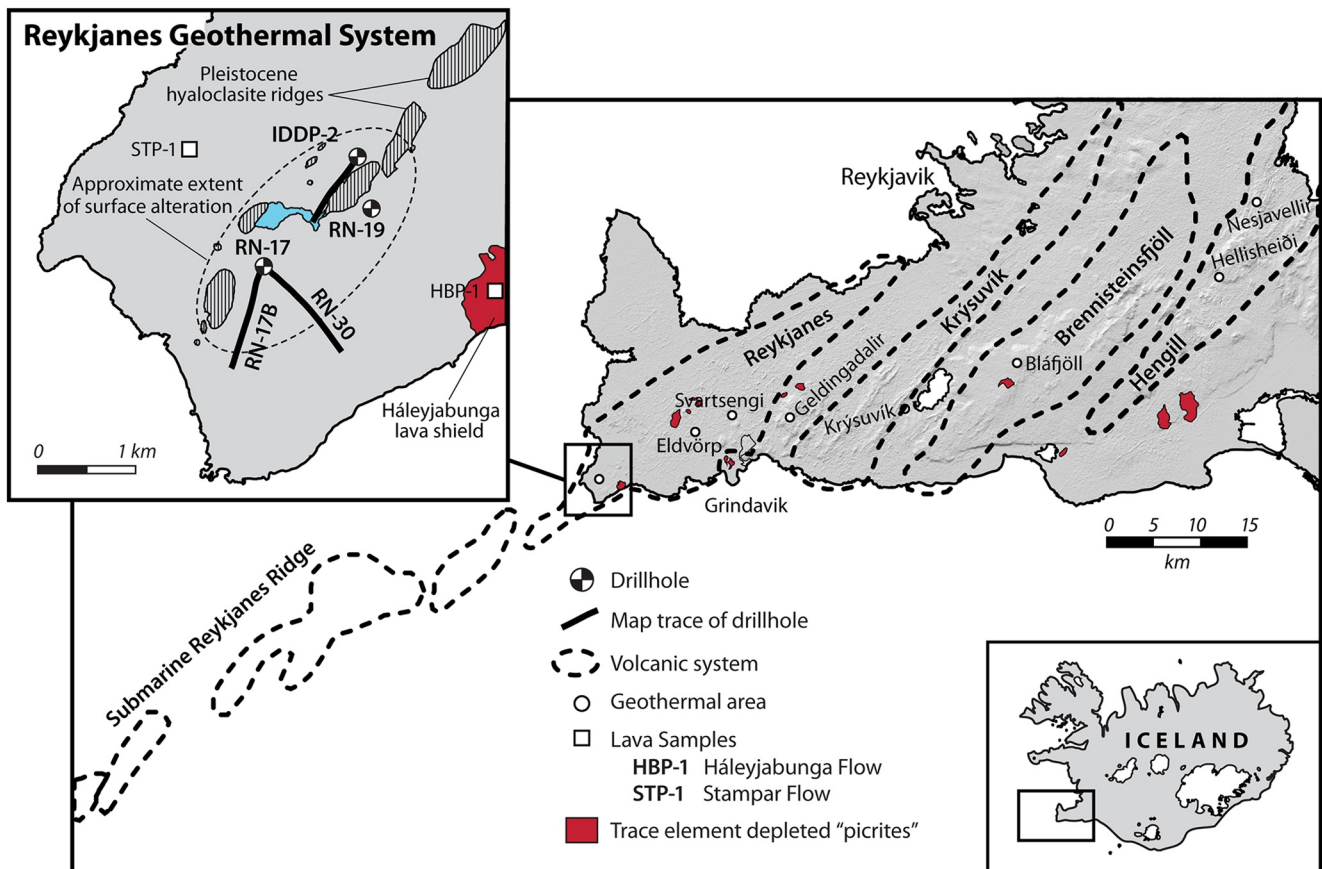
Figure 2. Location map of the Reykjanes Ridge, the northernmost section of the Mid-Atlantic Ridge, and the Reykjanes Peninsula showing an *en echelon* array of volcanic systems that accommodate spreading. The inset map shows the location of the Reykjanes geothermal field, including drill holes from which core samples have been recovered. Heavy dark lines extending from drill holes shows the surface trace of directionally deviated drill holes. Most of the surface of the Reykjanes Peninsula is covered by tholeiitic lavas and hyaloclastites belonging to the trace element enriched suite of Gee et al. (1998), including the Stampar Flow (STP-1) erupted around the year 1240. The location of the 2021 eruption in Geldingadalir is shown between the Reykjanes and Krýsuvík spreading segments. A sample of trace element depleted Háleyjabunga lava (HBP-1) was analyzed for comparison to the Stampar Flow and the drill core recovered from the IDDP-2 drill hole. Modified from Fowler and Zierenberg (2016) and references included therein.

smoker systems world-wide, it also forms massive sulfide deposits (scale) in drill holes and production pipes that resemble mid-ocean ridge volcanogenic massive sulfide deposits (Hardardóttir et al., 2009, 2010).

A key difference between the Reykjanes system and most mid-ocean ridge systems is the pressure control by water depth in the upper part of the hydrothermal system. Most seafloor vents occur at seawater depths greater than ~2 km, which are generally at pressures that prevent phase separation of venting fluid by boiling at the seafloor. Thus, single-phase high temperature fluids may be captured at the seafloor in gas-tight samplers that allow the total composition of the fluid to be analyzed in the laboratory facilitating reconstruction of the fluid properties at elevated temperatures (e.g. McDermott et al., 2018).

In production wells in the Reykjanes geothermal system boiling occurs down hole at a depth of ~1 km, at a pressure of ~40 bars, which is imposed by steam separators that feed the powerplant. Partitioning of acid generating gases into the steam phase forms an alkaline saline brine. The cooling and pH increase attendant on boiling results in supersaturation of metal sulfides. Full comparison of the composition of Reykjanes fluids to seafloor vent fluids collected prior to boiling therefore requires geochemical modeling to recombine the brine, vapor phases, and precipitated scale minerals to preboiling conditions (Fowler et al., 2019). Well fluids were collected below the boiling zone using down hole samplers in 2007 (Hardardóttir et al., 2009) and 2014 (Hannington et al., 2016). The downhole samples confirm that metal sulfide minerals precipitate in the boiling zone forming base metal and precious metal enriched well scale (Hannington et al., 2016; Hardardóttir et al., 2010).
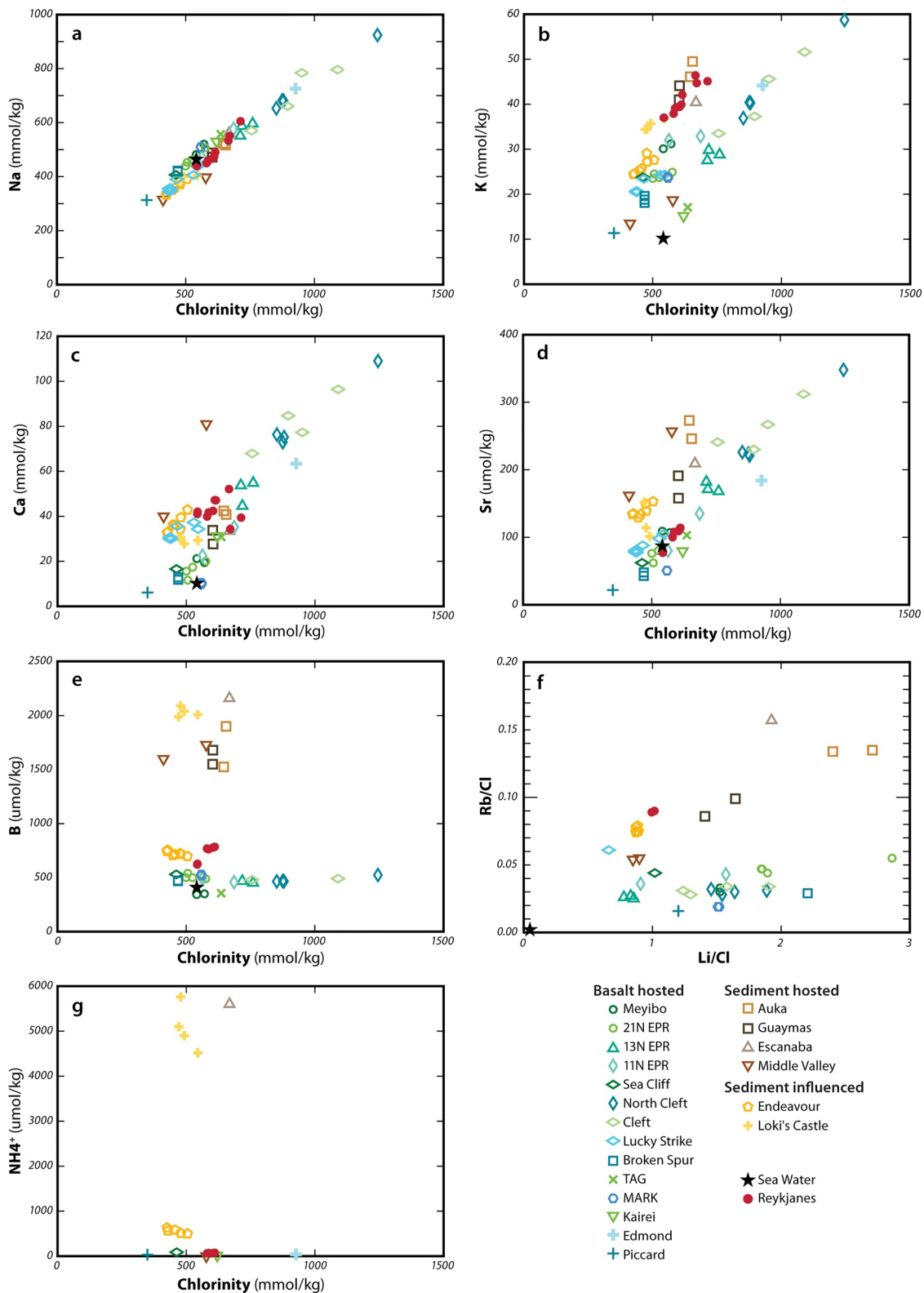
Figure 3. Comparison of Reykjanes geothermal fluid composition to seafloor hydrothermal fluids. (a) Na versus Cl. (b) K versus Cl. (c) Ca versus Cl. (d) Sr versus Cl. (e) B versus Cl. (f) Rb/Cl versus Li/Cl. (g) NH_4 versus Cl. Reykjanes fluids plot in the field of basalt-hosted geothermal system for most conservative elements but show a slight enrichment in B and alkali elements, similar to Endeavor Main Field samples from the Juan de Fuca Ridge, in the Pacific Northwest, Canada (Reykjanes data from Fowler et al. [2019], others from Paduan et al. [2018] and references contained therein).

With the exception of metal loss due to sulfide precipitation in the boiling zone, the reconstructed fluids collected at well heads and the fluids sampled downhole are similar in most respects to the black smoker systems, consistent with formation by seawater-basalt reactions at temperatures and pressures identical to the high temperature reaction zones that underlie normal mid-ocean ridges. Consequently, the Reykjanes system is an ideal natural laboratory to investigate seafloor hydrothermal systems by drilling without the technical challenges inherent in shipboard drilling. Another advantage is that more than 30 geothermal exploration, production, or injection wells, mostly in the depth range of 2 km, already existed in the Reykjanes geothermal field providing geologic context that is further constrained by geophysical survey data.

1.2. Drilling, Coring and Logging, IDDP-2

The drilling methods and parameters that were utilized in the IDDP-2 are described in Friðleifsson et al. (2017). A 2,500-m-deep pre-existing vertical production well (RN-15) was deepened to 2,750 m, and then directionally drilled along an azimuth of 210° at an initial inclination of 16° from vertical, which increased to approximately 36° at the bottom of the well. The hole was terminated at a down hole depth of 4,659 m. Down hole surveys place the base of the hole 738 m southwest of the RN-15 well head (Figure 2) at an elevation of ~4,450 m below sea level (Figure 1). The well was targeted to intersect a hydrothermal up-flow chimney identified by using drill hole temperatures and magnetotelluric data (Friðleifsson, Elders, et al., 2020).

Total circulation losses were encountered during drilling at 2.5–3.0 km depth and these continued to the final depth. These loss zones could not be sealed by addition of lost circulation materials, nor by multiple cement jobs. Consequently, no drill cuttings were recovered from the well deeper than these loss zones, except for the depth interval between 3.0 and 3.2 km (Friðleifsson, Albert, et al., 2020; Friðleifsson, Elders, et al., 2020). Consequently, the only rock samples recovered from 3.2 km to the total depth came from the 13 spot core runs that were attempted; the number of coring attempts was limited by the budget and time available. Four of these attempts were unsuccessful in recovering drill core.

A temperature/pressure log was measured in January 2017, after the well had been allowed to heat for only 6 days after drilling ceased (Friðleifsson, Elders, et al., 2020). This (T-P) log measured 426°C at 34.0 MPa at 4,560 m depth, close to the bottom of the well, conditions that are on the critical curve for sea water. This log also revealed the existence of a major zone of circulation loss/fluid entry at ~3,400 m, and smaller fluid flow zones at ~4,375 and ~4,500 m depths. At that time, the drill hole had not thermally equilibrated, and 40 L/s of cold, fresh surface water was being pumped into the top of the hole during the temperature run, so any measured temperature must be a minimal value. The pressure at the bottom of the hole was imposed by the level of water in the well which was balanced by the pumping rate of cooling water and the loss of fluid through the feed zones.

Prior to drilling it was not clear if basalt at 4.5 km depth would be at temperatures below the brittle-ductile transition for basalt, but the existence of the loss zones indicates that moderate to good permeability can exist, at least transiently, at these depths. A long-term project of injection of cold water into the well was carried out for several months in an attempt to enhance the deep permeability, and hopefully to permit production from the bottom of the hole (Friðleifsson, Albertsson, et al., 2020; Friðleifsson, Pálsson, et al., 2020). Unfortunately, this experiment was unsuccessful as the well became blocked due to partial collapse of the well casing. This also prevented logging of the deeper part of the well after it was allowed to heat up. At the time of submission of this paper, attempts to flow the well and sample deep hydrothermal fluid have not been successful (Friðleifsson, Albertsson, et al., 2020). This meant that rather than relying on direct downhole measurements, detailed studies of the drill core were the chief means of understanding the conditions in the HTRZ. The drill core provide insight into the evolution of the deep geothermal system.

2. Drill Core Analytical Methods

Four-inch (~10.16 cm) diameter spot cores were recovered from six depth intervals between 3,648 and 4311.2 m down hole with variable to poor core recovery; 22.16 m of 2.625-inch (~6.68 cm) diameter core was recovered at the bottom of the hole between 4634.2 and 4,659 m (89% recovery). Detailed core descriptions and graphic logs are provided in Text S2 of Supporting Information S1. Intact intervals of core were
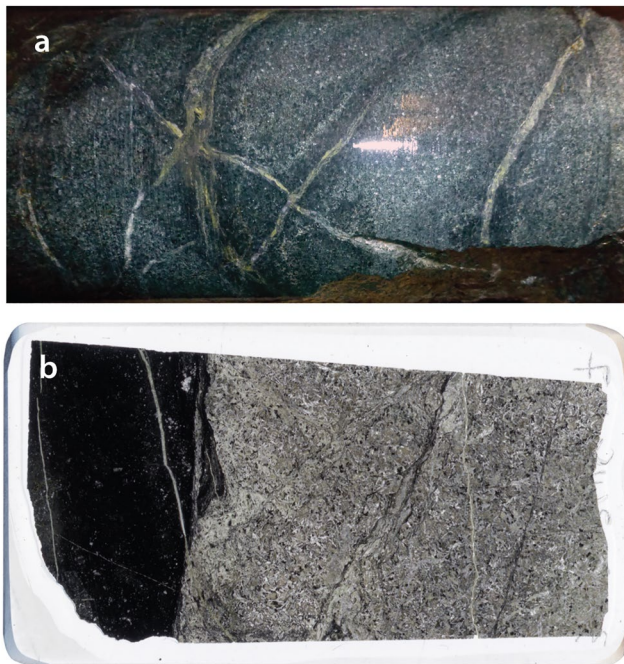
Figure 4. (a) Four-inch diameter drill core from 3,648 m depth, Core 3, showing cross-cutting plagioclase-epidote-amphibole-quartz veins, with dark chlorite-magnetite-rich selvages. (b) Scanned thin section (2.5 by 4.5 cm) showing dark chilled margin of younger, overlying dike (to left) against fine-grained diabase with plagioclase-epidote veins (3648.47 m). Thin veins cutting chill margin (top left to bottom right) are primarily filled with hydrothermal clinopyroxene which changes to dominantly amphibole passing into the crystalline diabase.

photographed and logged (density, natural gamma activity, magnetic susceptibility) with a GEOTEK multisensor core logger (Mesfin et al., 2020). Thirty-seven samples were examined using transmitted and reflected light petrography of polished thin sections. Most samples were also examined by secondary electron and back scatter electron microscopy on a Cameca SX-100 electron microprobe (EMP) equipped with an energy-dispersive spectrometer. The detailed examination of the core and polished thin sections are the fundament constraints upon which the inference about geologic processes presented in this paper are based. Due to constraints on publication length, much of the documentation of mineralogy, textures and paragenetic relationships are presented in Supporting Information S1 archived with this publication. The necessity of presenting this material in this manner in no way diminishes its importance, and interested readers are encouraged to view this information.

Quantitative mineral chemistry was obtained using the same instruments and following the techniques described in Fowler et al. (2015) and Schiffman et al. (2014). Titanium content in quartz was determined by EMP at the University of Oregon using the methods of Acosta et al. (2020). Twenty-one core samples were selected for bulk rock geochemical analysis at the Washington State University Geoanalytical Laboratory, following methods described in Fowler and Zierenberg (2016). At the same time, unaltered samples of the Stamper lava and the Háleyjabunga lava shield were analyzed for comparison.

3. Drill Core Data and Observations

Preliminary descriptions of the core samples recovered from the IDDP-2 drill hole are provided by Friðleifsson et al. (2017), Zierenberg et al. (2017), Friðleifsson, Elders, et al. (2020), and Zierenberg et al. (2020). The dominant lithology recovered in all of the cores is fine- to coarse-grained diabasic dikes from a sheeted dike complex. Primary igneous textures are generally well preserved, but the rocks are pervasively hydrothermally altered and thoroughly recrystallized. All of the diabases have the same primary mineralogy of plagioclase-augite-titanomagnetite with the exception of the uppermost dike (Dike 1) in Core 11 (~4,635 m) which has sparse (<1%) phenocrysts of olivine (Text S2 in Supporting Information S1). This work provides the first detailed description of the mineralogy, mineral paragenesis, mineral chemistry, and bulk rock chemical data from these cores. The results are presented in order of increasing depth down hole with a description of bulk rock composition, petrography, mineralogy, and mineral chemistry followed by a discussion of the implications of these results for understanding seawater-basalt alteration in mid-ocean ridge hydrothermal systems and ophiolites, including the role of supercritical fluids in the deep high temperature reaction zone. The results are organized by similarity of alteration mineral assemblages into three zones: Geothermal Reservoir Transition Zone, Hornblende Zone, and Pyroxene Zone.

3.1. Geothermal Reservoir Transition Zone

3.1.1. Core 3 (3068.7–3074.1 m)

The rocks recovered in Core 3 (Figure 4) contain portions of three dikes separated by two chilled margins. In each case the shallower overlying dike is chilled against the older underlying dike. The glassy/cryptocrystalline quenched margins are approximately 1 cm thick. Subophitic igneous texture is well preserved. Plagioclase is cloudy but retains its primary crystal outline and zoning patterns. Pyroxene is extensively replaced by amphibole, but pyroxene that has the appearance of primary igneous augite remains. Titanomagnetite has poorly preserved oxidative exsolution texture and is partly altered to magnetite with minor hematite and fine-grained titanite replacing some of the ilmenite laths.

The Core 3 samples have the lowest contents of SiO_2, Zr, Fe, Ti, Na, and K, and highest Mg and Ca contents among the diabases (Table S1 in Supporting Information S1; Figure 5). The Core 3 samples are transitional between Trace Element Enriched (TEE) and Trace Element Depleted (TED) basalt types on a plot of Zr normalized Y versus Nb (Figure 5h). They are also the only diabase samples that show some depletion in the light Rare Earth Elements (REE), again transitional between TEE and TED basalts (Figure 5g).

Samples from Core 3 are the only rocks that have the same mineral assemblage as the overlying geothermal production reservoir: plagioclase, hornblende, actinolite, epidote, chlorite, diopside, quartz, magnetite, ilmenite, titanite, isocubanite-chalcopyrite, pyrite, pyrrhotite, and trace sphalerite. Plagioclase is extensively altered, but generally retains its igneous morphology. Pyroxene is nearly completely replaced, generally by amphibole, but also by chlorite in areas adjacent to veins. Much of the amphibole has the fibrous habit of actinolite, but the optical properties of hornblende. Coarser grained subhedral to euhedral blocky hornblende overgrows and replaces fibrous amphibole.

The core is extensively veined (Figure 4a), but in contrast to shallower reservoir rocks, sharp-walled, open-space filling veins are absent. The hydrothermal veins are centimeter-scale, discontinuous, anastomosing replacement veins dominated by plagioclase, amphibole, epidote and quartz. These veins generally have darker selvages that are best developed at vein intersections (Figure 4a), which are chlorite-rich with abundant very fine-grained disseminated magnetite. Less abundant, early, nearly monomineralic millimeter-scale veins of amphibole and hydrothermal clinopyroxene that crosscut the chilled margins change from clinopyroxene dominated in the chilled zone to amphibole dominated in the crystalline portion of the dike (Figure 4b). Based on cross cutting relationships, the paragenetically latest veins are mm-scale plagioclase-amphibole veins and later hornblende veins, both of which lack chlorite and epidote.

Plagioclase in Core 3 is on average more calcic than any of the deeper cores (Table S1 and Figure S1a in Supporting Information S1) and there is no systematic difference in composition between altered igneous plagioclase and hydrothermal plagioclase in the matrix or veins. Plagioclase is more calcic than typical diabasic plagioclase with a mean anorthite number (An#) of 88.6. Hydrothermal plagioclase can be distinguished from igneous plagioclase by lower concentrations of trace elements such as Mg and Fe (Table S2 in Supporting Information S1) (Marks, Schiffman, Zierenberg, Elders, et al., 2010; Zierenberg et al., 2017). Median concentrations of MgO, FeO, and K_2O are 0.016, 0.35, and 0.018 wt.%, respectively.

Hydrothermal clinopyroxene in veins is also distinctly calcic (mean Ca/Ca + Mg + Fe (Wo) = 0.49) and plots along the diopside-hedenbergite join (Table S3 and Figure S1b in Supporting Information S1). Interestingly, residual igneous clinopyroxene is also more calcic than typical igneous augite and overlaps the composition of pyroxene in hydrothermal veins. The mean magnesium number (Mg#) is 62.4. Clinopyroxene has lower concentrations of Al_2O_3 (mean 2.0 wt.%) compared to igneous augite and has low concentrations of trace elements with median values TiO_2, Na_2O, and Cr_2O_3 of 0.30, 0.07, and 0.01 wt.%, respectively (Table S3 in Supporting Information S1).

Amphibole compositions show a range from actinolite to aluminous hornblende (Figure S1c in Supporting Information S1) with most values falling in the hornblende field. There is no clear systematic difference in composition of amphibole replacing augite, in the rock matrix or in hydrothermal veins. Amphibole has an average Mg# of 66 and Cl content of 0.1 wt. % (Table S4 in Supporting Information S1).

3.2. Hornblende Zone

Rocks recovered in Cores 5 through 10 (3865.5–4311.2 m) share similar alteration characteristics and are described below by increasing depth. In general, each core recovered from the Hornblende Zone is from an interior portion of a single diabasic dike, ranging from fine-grained to medium-grained diabase, but some small intervals of felsic rock, the first recovered from the Reykjanes geothermal field, are also present (Table S1 in Supporting Information S1).

3.2.1. Cores 5 and 6 (3865.5–3870.2 m)

Core 5 recovered 3.85 m of continuous core, with no missing intervals or coring gaps, plus 0.15 m of the same intrusion in Core 6. The recovered core is a relatively homogeneous dark greenish gray basaltic intrusion (Figure 6a). The protolith was composed of subequal amounts of euhedral, clear, blocky to slightly
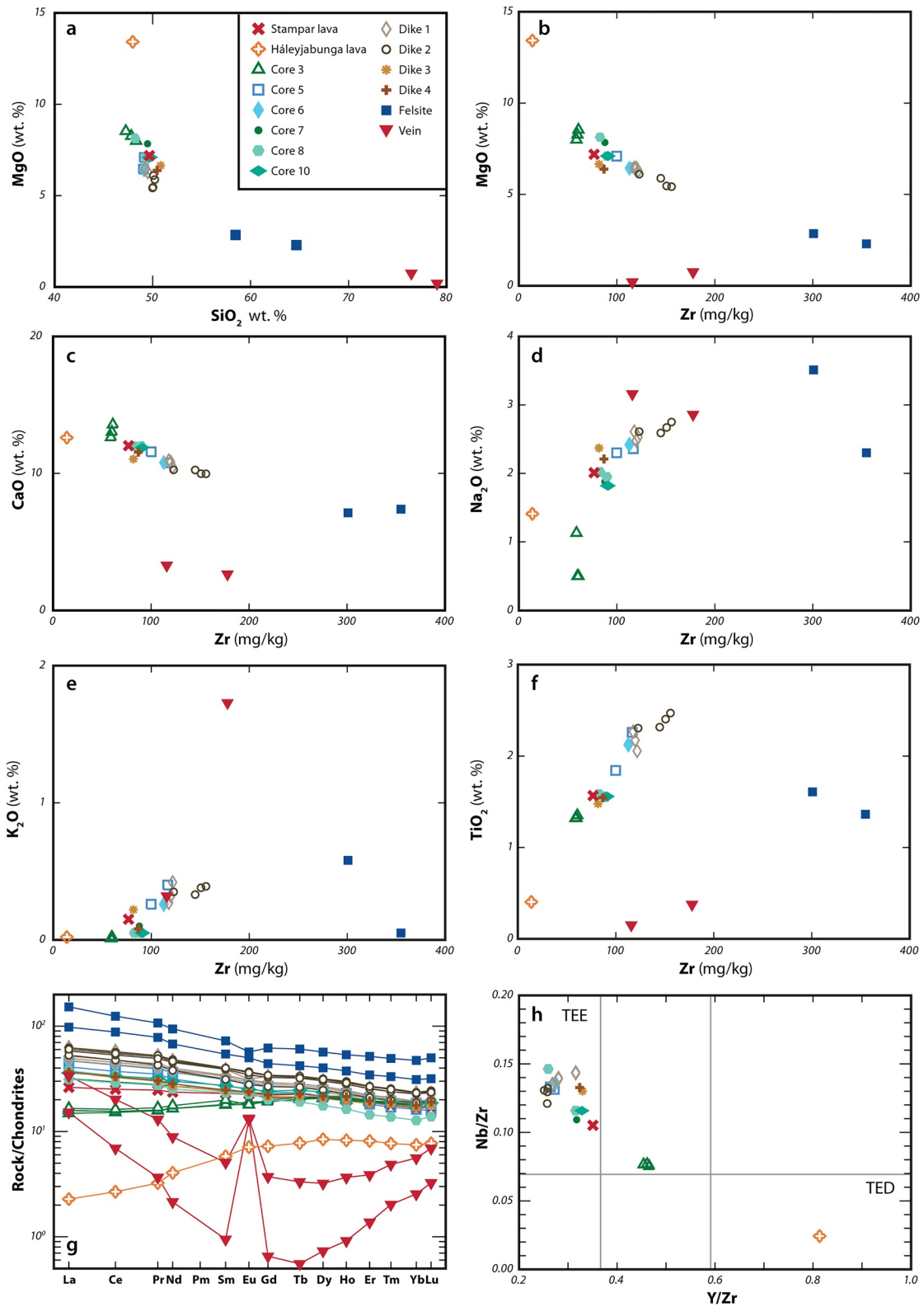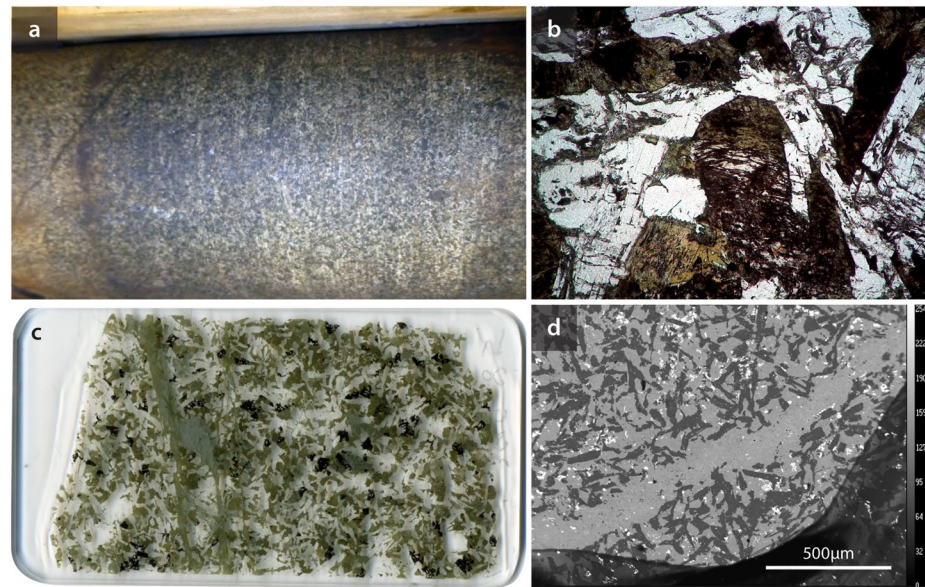
Figure 5.

Figure 6. (a) Four-inch diameter drill core from 3,869 m depth, Core 5, showing homogeneous medium-grained diabase. Only rare, mm-scale hornblende veins are present, such as the NE-SW trending dark vein on the left edge of the image. (b) Photo micrograph in plane polarized light (ppl) showing dusty plagioclase and augite replaced by hornblende (3865.50 m; Field of view = 2.1 mm). (c) Scanned thin section (2.5 by 4.5 cm; 3869.85 m; Core 6) showing preservation of igneous texture despite pervasive alteration of the plagioclase (clear) and replacement of the augite by hornblende (green). Opaque grains are titanomagnetite. Near vertical branching hornblende replacement vein on left side of the image. (d) Electron backscatter image (EBS) showing euhedral plagioclase (darkest gray) and interstitial augite replaced by hornblende, with a thin (<100 μm) hornblende vein cutting from lower left to upper right. Brightest phase is titanomagnetite. (4254.83 m, Core 8).

elongate 3–5 mm plagioclase with interstitial subhedral to euhedral 2–3 mm augite, and approximately 5%–8% euhedral, 2 mm, titanomagnetite. Augite is pervasively altered to hornblende and only small patches of residual augite remain. Plagioclase and titanomagnetite generally retain their igneous morphology but are also extensively altered. A few slightly lighter, cm-scale bands in the core are distinguished by a very slight increase in modal plagioclase and the occurrence of some patches of myrmekitic intergrowth of quartz and intermediate plagioclase.

The near total lack of secondary mineral veining in this section of core is notable. There are a few <1 mm hairline veins of dark green to black amphibole that cut the core at various angles (Figures 6a and 6c), with large changes in vein direction along a single vein. Overall, the rock appears relatively tight and impermeable despite the fact that alteration of both augite and plagioclase is pervasive. Secondary sulfide minerals include pyrite, which is more common in the myrmekitic zones, pyrrhotite, and isocubanite with exsolved chalcopyrite lamellae.

3.2.2. Core 7 (4089.5–4090.6 m)

Core 7 recovered a small interval of broken core pieces representing the interior portion of a diabase dike. The protolith was similar in composition and texture to the dike recovered in Cores 5 and 6 but is somewhat finer-grained. The alteration assemblage is also similar to that in Cores 5 and 6, but the alteration is more extensive with patchy recrystallized zones of intergrown hornblende and plagioclase. Cummingtonite is

Figure 5. Compositional trends from IDDP-2 samples compared to representative samples of the two major lava series (Gee et al., 1998), trace element enriched (TEE, Stampar lava) and trace element depleted (TED), Háleyjabunga lava. (a) Mg versus SiO_2. (b) MgO versus Zr. (c) CaO versus Zr. (d) Na_2O versus Zr. Diabases and felsites generally fall along a differentiation trend consistent with TEE lavas, but quartz-rich felsic vein samples do not. Core 3 diabases appear to have lost Na_2O during hydrothermal alteration. (e) K_2O versus Zr. (f) TiO_2 versus Zr. (g) Chondrite normalized (Sun & McDonough, 1989) REE. (h) Nb/Zr versus Y/Zr. Felsites have low TiO_2 contents, but have REE values consistent with differentiation from diabase, whereas the more silica-rich felsic veins have REE patterns that match hydrothermal fluids. Nb, Y, and Zr values separate the diabases into the TEE group, with those from Core 3 transitional to TED.

present in trace amounts in some samples and is more manganese-rich compared to co-existing hornblende (Table S4 in Supporting Information S1). Pyrrhotite and isocubanite are present in trace amounts, and locally intergrown with pyrite.

3.2.3. Core 8 (4254.6–4255.3 m)

Drilling rubble, referred to here as "rollers," was recovered on top of several of the cores. One sample, (Roller A in Table S1 in Supporting Information S1; sample 4250 on figures), was selected for chemical and petrographic analysis as it was the least altered sample of diabase recovered from down hole. Although the depth from which this sample is derived can only be constrained between the bottom of the casing at ~3,000 m and the top of the core at 4254.6 m, the lack of similar unaltered fragments overlying shallower cores suggest that this fragment was likely derived from the interval between the bottom of Core 7 (4090.6) and the top of Core 8.

Roller A was derived from the interior of a coarse-grained diabase dike with approximately 60% euhedral plagioclase up to 4 mm in length separating blocky pyroxene (Figures S2a and S2b in Supporting Information S1). Titanomagnetite is abundant, ~5%, and shows well developed oxidative exsolution of ilmenite from magnetite.

Pyroxene shows incipient alteration to hornblende, and less commonly actinolite, along grain boundaries. Plagioclase shows only limited patchy alteration to more albitic compositions, generally along cracks. Unaltered plagioclase phenocrysts show a narrower range of An# (63.4–76.9) and have MgO contents that systematically increase, and K_2O and Fe_2O_3 contents that decrease, with increasing An# (Table S2 in Supporting Information S1). Unaltered augite also shows a narrow range of Mg# (67.8–76.9), elevated TiO_2, Al_2O_3, Na_2O, and reduced MnO compared to most hydrothermal pyroxene (Table S3 in Supporting Information S1).

Core 8 had poor recovery of a fine-grained basaltic intrusion, including poorly preserved portions of a quenched dike margin. The rock has an ophitic texture with maximum grain size of plagioclase laths of approximately 250 μm, with the exception of one sample that included a xenocryst aggregate of plagioclase crystals up to 2 mm. The An# and trace element concentrations of the xenocrysts overlap with those of unaltered plagioclase phenocrysts analyzed in Roller A (Table S2 in Supporting Information S1).

Samples from Core 8 are the most intensely veined and deformed samples recovered from the Hornblende Zone. No residual igneous pyroxene remains due to the pervasive alteration to amphibole. Several generations of plagioclase-hornblende-magnetite ± quartz ± isocubanite-chalcopyrite ± pyrite veins are present. Euhedral biotite is present in one vein. The finer-grained portions of the rock are brecciated along some vein margins and have locally developed a foliation defined by elongate amphibole grains. Titanite is commonly observed and trace amounts of cummingtonite are present in the matrix alteration (Table S4 in Supporting Information S1).

3.2.4. Core 10 (4309.9–4311.2 m)

Core 10 recovered three half round core pieces that are bounded on one side by a drilling-induced fracture that is approximately in the plane of the core axis. The protolith had subequal amounts of plagioclase and augite grains up to 2 mm in size, but augite has been completely replaced by amphibole. Feldspar grains tend to be cloudy white to a light bluish green in thin section. Titanomagnetite is more abundant (~7%) in this dike, occurring as 1 mm anhedral grains. Oxidative exsolution of ilmenite from magnetite is common, but in contrast to overlying rocks, the lattice pattern of exsolution is less distinct and some grains have started to recrystallize to blebby intergrowths that poorly mimic the original exsolution texture.

The core is locally cut by plagiogranite segregation veins, the thickest of which is a 2 cm wide band dipping at approximately 70° to the core axis (Figure S2c in Supporting Information S1). The drill hole was inclined by about 30° from vertical at this depth, so the felsic band could have originally been approximately horizontal, but the core is not oriented. Prior to this, felsic rocks have not been reported from the Reykjanes Peninsula. The plagiogranite is approximately 70% feldspar, most of which is anhedral and cloudy white. However, there are some euhedral, 2 mm blocky plagioclase crystals that are relatively clear and glassy. The plagiogranite contains some elongate, 3–4 mm long prismatic grains that appear to have been pyroxene, based on their morphology (Figure S2d in Supporting Information S1), that has been replaced by hornblende. Much of the hornblende in the plagiogranite is fine-grained and anhedral and appears to be inherited from the

altered diabase along with disseminated titanomagnetite. The boundaries of the plagiogranite vein with the wall rock are diffuse and somewhat gradational. Healed fractures cutting through some of the plagiogranite may have a small amount of subhedral gray quartz along the vein trace, but otherwise quartz is a very minor phase. Apatite is a common accessory mineral and a minor amount of disseminated fine-grained sulfide is present, mostly Cu-Fe sulfide. A sample from 4310.06 m contains pyrrhotite intergrown with subhedral pyrite, the deepest occurrence of pyrite observed.

A sample of the plagiogranite vein was separated for bulk chemical analysis. The sample is a dacite (64.57% SiO_2) and has concentrations of Al_2O_3, MgO, CaO, Sc, Nb, Hf, Ta, U, Th, and REE that plot approximately along the extension of the apparent differentiation trend defined by the diabases (Figure 3). Na_2O, K_2O, FeO, and TiO_2 plot at values lower than would be expected from continuation of the trend of the diabasic rocks. Total REE are elevated relative to the diabase but have a similar chondrite normalized pattern (Figure 5g).

3.2.5. Mineral Chemistry

Histograms of plagioclase compositions (Table S2 in Supporting Information S1) for Cores 5,6,7,8 and 10 are shown in Figure S3 of Supporting Information S1. Igneous plagioclase in the least altered sample (4250) and xenocrystic plagioclase in a sample from 4254.83 m have a relatively narrow range of compositions with an average An# of 71.8 (±5.9). Plagioclase in the Hornblende Zone is less calcic than in the overlying Geothermal Reservoir Transition Zone (Figure 7a). Despite the broad distributions at each depth level, the An# of replaced igneous plagioclase and hydrothermal plagioclase in the matrix increases down hole. Plagioclase in veins overlaps in composition with matrix plagioclase. Symplectic plagioclase in the lighter colored bands in Cores 5 and 6 has an average An# of 18.8 (±11); plagioclase in the felsite band in Core 10 has an average An# of 49.9 (±12.5).

Amphibole compositions (Table S4 in Supporting Information S1) span the range from actinolite to hornblende with some samples from the shallowest two cores extending into the edenite field (Figure S4 in Supporting Information S1). There is no systematic variation in the tetrahedral aluminum (IV Al) content with depth (Figure 7b). Actinolite and hornblende are intergrown at fine scales and there is no apparent paragenetic distinction based on the observed mineral textures and cross cutting relationships.

Pyroxene compositions for the least altered diabase (4250), and rare residual pyroxene in the altered diabases, plot in the augite field (Table S3 and Figure S5 in Supporting Information S1). A single occurrence of hydrothermal clinopyroxene (3869.52 m) shows higher Ca and Fe concentrations compared to augite (Figure S5 in Supporting Information S1). The composition of clinopyroxene from Cores 5, 6, and 7 overlaps the composition of augite in the least altered diabase including high values of Al_2O_3, TiO_2, and Na_2O, relative to pyroxene in the underlying Pyroxene Zone, and we interpret these as residual patches of igneous augite remaining after most augite has altered to hornblende. No residual igneous pyroxene was observed in Cores 8 or 10.

3.3. Pyroxene-Zone

Cores 11–13 (4,634–4,657 m) were recovered from the bottom of the hole using a different coring system with a smaller diameter which resulted in improved core recovery (Friðleifsson et al., 2017). As a result, we have a nearly continuous 23 m record of the deep alteration in the hydrothermal up-flow zone that feeds the Reykjanes geothermal system (Friðleifsson, Elders, et al., 2020). Portions of four diabase dikes were recovered separated by three chilled margins quenched against the interior portion of a split dike. The quench margins are much thinner (1–2 mm) than those from the more shallowly emplaced dikes recovered in Core 3. In each case, the shallower dike was chilled against (was younger than) the underlying dike. The dikes are described from shallowest (youngest) to deepest (oldest) and are referred to as Dike 1 to 4, respectively. All of the dikes share the same alteration history which is characterized by the ubiquitous presence of hydrothermal clinopyroxene and orthopyroxene in addition to plagioclase, hornblende, magnetite, and ilmenite that characterizes the overlying Hornblende Zone. Apatite is a ubiquitous accessory mineral along with isocubanite-chalcopyrite and in a few samples, minor amounts of pyrrhotite. There is no indication that rocks have gained phosphorous (Table S1 in Supporting Information S1), rather recrystallization of plagioclase has likely allowed apatite to grow into more easily recognized mineral inclusions.
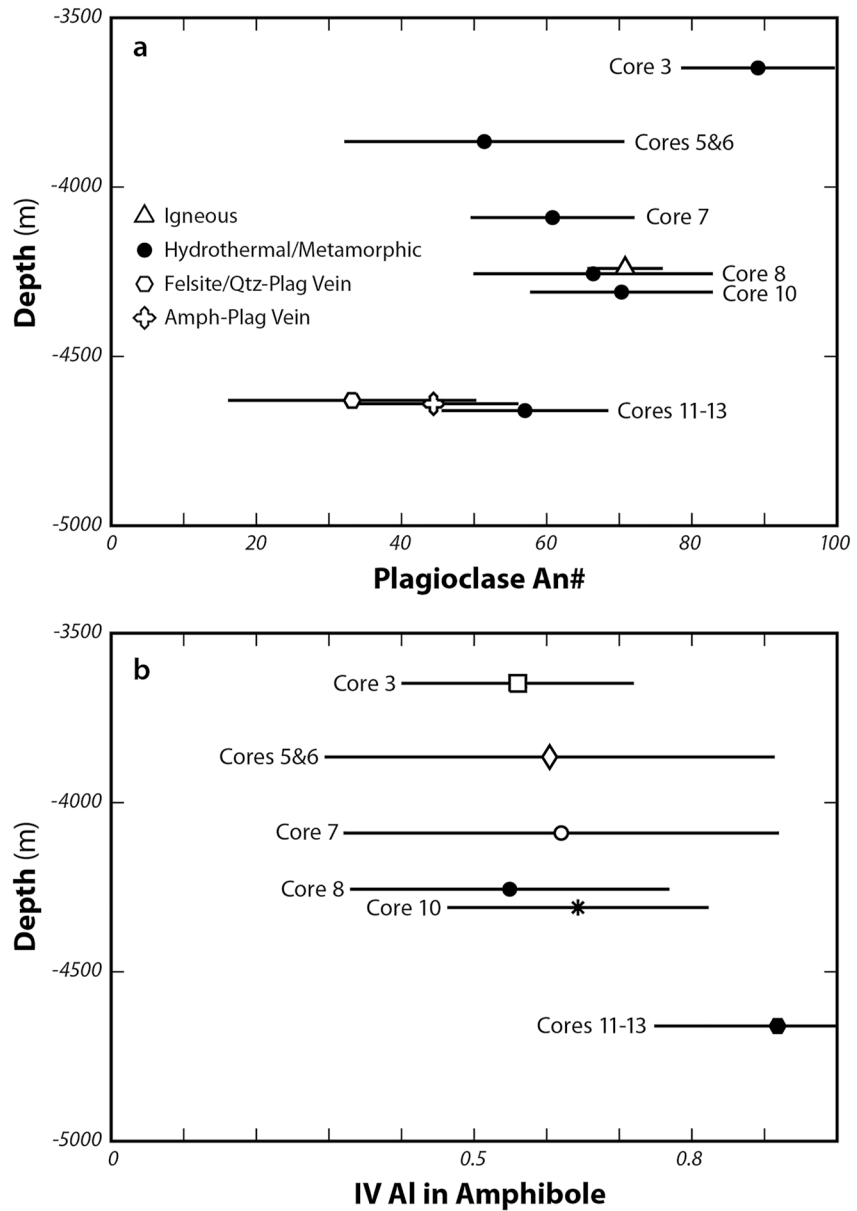
Figure 7. Down hole changes in mineral composition. (a) Plagioclase An# versus depth (m) (b) Tetrahedral aluminum (IV Al) in amphibole versus depth (m).

3.3.1. Dike 1 (4634–4635.35 m)

Dike 1 shows a sharp chilled margin against dike two with 1 mm elongate plagioclase phenocrysts that are flow aligned parallel to the dike margin (Figures S6a and S6b in Supporting Information S1). The degree of flow alignment decreases away from the chilled margin and the phenocrysts coarsen to approximately 5 mm in the dike interior. The plagioclase phenocrysts generally retain twinning and weakly developed growth zoning patterns typical of igneous plagioclase, but they are somewhat dusty looking due to an abundance of very fine-grained to microscopic fluid/vapor inclusions and abundant needles and blebs of apatite. Augite was interstitial to plagioclase but is now an intimately intergrown mixture dominantly composed of hornblende with orthopyroxene, clinopyroxene and biotite (Figure S6c in Supporting Information S1). Orthopyroxene is more abundant than clinopyroxene. The mafic minerals are intergrown at all scales from the size of the original augite down to the limits of resolution. The original rock contained sparse phenocrysts of 3 mm euhedral olivine, most of which has been pseudomorphed by a mixture of mafic alteration

minerals. Rounded cores of remaining olivine are replaced and mantled by orthopyroxene (Figures S7a and S7b in Supporting Information S1). Titanomagnetite was disseminated throughout the rock, but in contrast to overlying dikes in the Hornblende Zone, magnetite and ilmenite do not retain their original lattice-controlled oxidative exsolution texture, but rather occur as equant to rounded grains. Groundmass alteration is a mixture of plagioclase, hornblende, orthopyroxene, clinopyroxene and biotite with minor quartz. Pyrrhotite and isocubanite/chalcopyrite are present in minor but variable amounts.

3.3.2. Dike 2 (4635.35–4650.70 m)

Dike 2 has an equigranular texture with plagioclase interstitial to augite and abundant (5%–7%) disseminated equant titanomagnetite. Plagioclase and pyroxene grain size gradually increases down core to ~2–3 mm at approximately 4,642 m and then gradually decreases to the chilled margin quench against the underlying dike. In contrast to the dike above, the chilled margin of Dike 2 is irregular with thin stringers of Dike 2 melt intruding into Dike 3 (Figure S8 in Supporting Information S1). Small fragments and partially disaggregated crystals of Dike 3 are incorporated into the chilled rock suggesting that the crystalline interior of Dike 2 may not have been completely solidified. One sample of Dike 2 (4649.73 m) has plagioclase xenocrysts up to 6 mm in length with a clear core overgrown by a more inclusion-rich zone itself overgrown by a thin clear rim (Figure S8d in Supporting Information S1). A nearby sample (4650.67 m) has a large (8 mm) xenocryst of enstatite, the only occurrence of igneous orthopyroxene documented from the IDDP-2 cores (Figure S8e in Supporting Information S1).

Groundmass alteration is similar to that described for the overlying dike. Plagioclase generally retains its igneous morphology, but it contains abundant fluid/vapor inclusions. Augite is completely replaced by hornblende that is intimately intergrown with orthopyroxene, clinopyroxene and biotite, which is more abundant in Dike 2. Titanomagnetite and ilmenite have recrystallized metamorphic textures similar to Dike 1.

3.3.3. Dike 3 (4650.70–4652.05 m)

Dike 3 is a medium to fine grained intrusive with a heterogeneous texture. Irregular centimeter-scale patches of coarser-grained (~4 mm) diabase are dispersed through the finer-grained (2–3 mm) diabase. The coarser patches appear to have more original pyroxene and titanomagnetite compared to the finer-grained matrix. There is a sharp chilled contact with the underlying dike. The chilled margin has sparse 1–4 mm plagioclase phenocrysts that are not aligned with the dike margin.

Alteration in Dike 3 is similar to that described above, but the grain-size of secondary clinopyroxene and orthopyroxene are generally coarser. Disseminated biotite is present in the shallowest portion of the dike, down to ~4,651 m, but is not present in deeper sections. The presence of biotite alteration is coincident with a zone of elevated natural gamma intensity recorded by a multisensory core logger (Mesfin et al., 2020).

3.3.4. Dike 4 (4652.05–4657.58 m)

Dike 4 is similar to Dike 3 but is more feldspar rich and has a more heterogeneous texture with irregular gradations between coarser and finer grained patches. Glomerocrysts of 3–4 mm blocky plagioclase with interstitial augite grade into a more felted textured matrix with 2–3 mm plagioclase laths.

Matrix alteration is similar to the overlying rocks, except for the lack of biotite. Locally, mm scale bands of well-developed granoblastic pyroxene are present (Figures S9a and S9b in Supporting Information S1). These areas are rich in hydrothermal clinopyroxene with less abundant orthopyroxene and sparse interstitial amphibole and plagioclase. These zones grade into the typical plagioclase-hornblende-clinopyroxene-orthopyroxene assemblage that preserves original igneous texture. The granoblastic zones are present in the coarser interior of the dikes and are not observed next to chilled margins of adjacent dikes, as might be expected if they formed by contact metamorphism. In one section (4654.16 m), a granoblastic textured clinopyroxene band is in contact with a parallel band of fine-grained equigranular textured anorthite (Figure S9c in Supporting Information S1) indicating the onset of segregation veining similar to that which characterizes high grade mafic gneisses.

Thin, early, high temperature plagioclase-quartz veins cut the rock at various angles (Figure S9e in Supporting Information S1) (4655.99 m). Quartz is generally absent to rare as a matrix alteration mineral in the overlying rocks but is present as interstitial aggregate patches in the rocks that show the most extensive

Figure 8. (a) Altered diabase drill core from Dike 1 at 4634.5 m depth (2.625 inches diameter) showing early dark hornblende (±plagioclase) veins cut by a later felsic vein (with reddish-orange iron surface staining). This sample is unusual in the density of veins, which are generally quite sparse, much fewer than 1 vein per meter. The iron staining that shows best on the white felsite vein is an artifact formed during the coring process by interaction with drilling fluids. (b) Patch of plagiogranite with irregular margins with the altered diabase of Dike 2 (4650.67 m). (c) Late-stage quartz-rich felsic vein cutting altered diabase of Dike 1 (4635.11 m). Yellow staining formed after cutting the core due to K-Fe-Cl salts precipitated after evaporation of interstitial pore fluid.

metamorphic recrystallization. A 1.5 by 0.5 mm irregular pod filled mostly by medium to coarse grained polygonal quartz is present in one of the deepest samples (Figure S9e in Supporting Information S1) (4655.99 m). The walls of the quartz-filled pod are partly lined by a layer of myrmekitic quartz-plagioclase with the texture of a quenched eutectic liquid (Figure S10 in Supporting Information S1). Dendritic to plumose growths of skeletal plagioclase in optical continuity, intergrown with quartz in optical continuity, coarsen and fan out into the interior of the pod. The fronts of these eutectic plumes are subsequently overgrown by polygonal quartz, which is coarsest grained in the interior of the pod. An approximate bulk composition of this quenched incipient melt pocket was obtained by averaging 75 10 µm raster electron microprobe analyses across the quartz-plagioclase intergrows, which are presented in Table S5 of Supporting Information S1 and discussed in a subsequent section of the paper.

3.3.5. Hornblende Veins and Felsic Segregations/Veins

The material recovered in Cores 11–13 is notable for the general lack of hydrothermal veining. Figure 8a is uncharacteristic in that it contains several veins, but it illustrates two prominent types of hydrothermal replacement veining observed at the bottom of the hole. A single open fracture partially filled by minerals growing into open space recovered at 4337.80 m is the paragenetically latest phase of hydrothermal activity recorded in the core.
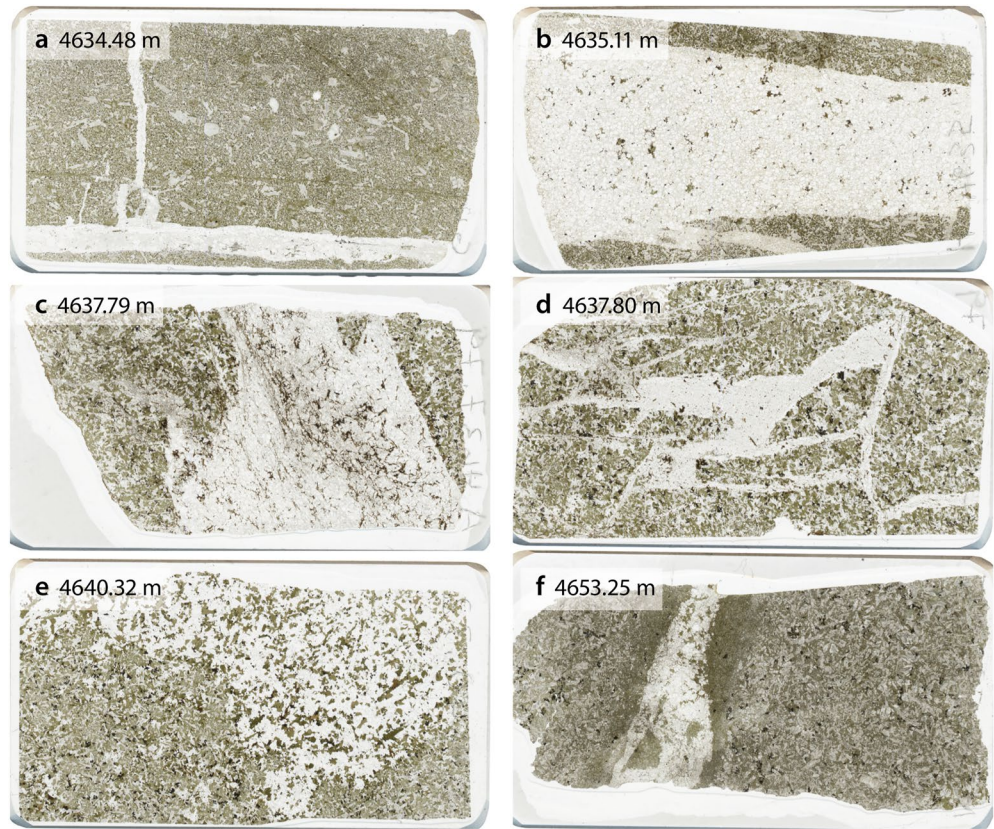
Figure 9. Scanned thin sections (2.5 by 4.5 cm) of various textures of felsic segregations and quartz-rich plagioclase veins. (a) Thin sharp walled, branching and intersecting quartz-plagioclase veins (4634.48 m, Core 11). (b) Quartz-plagioclase composite vein with plagioclase-rich margins and quartz-rich center (4635.11 m, Core 11). (c) Irregular replacement vein with coarser-grained euhedral plagioclase-rich margin on the right and sugary quartz-rich left margin (4637.79 m, Core 11). (d) Felsic vein breccia network (4637.80 m, Core 11). (e) Irregular patch of plagiogranite with diffusive contacts with the diabase (4640.32 m, Core 11). (f) Quartz-plagioclase vein with inclusions of wall rock and dark, fine-grained hornblende-rich vein selvages (4653.25 m, Core 13).

The earliest phase of veining is dominated by hydrothermal amphibole, often as monomineralic replacement veins (Figure 8a). These range from less than 1 to ~5 mm in thickness and cut through the rock without well-defined vein walls. They replace diabase matrix, plagioclase phenocrysts, and altered augite. Millimeter-scale through-going amphibole veins often have poorly defined darker selvedges characterized by a higher proportion of amphibole, relative to pyroxene in replaced augite. Hornblende-only veins occasionally intersect with no offset. Amphibole-plagioclase veins are less abundant than amphibole only veins and vary from amphibole-rich to plagioclase-rich. The plagioclase-rich replacement veins are anastomosing and discontinuous. Quartz is present in the hornblende-plagioclase and plagioclase veins from the deepest cores, and orthopyroxene is present in at least one vein (4651.10 m).

The most prominent "veins," although still a minor (<1%) component of the rock, are felsic plagiogranite segregations and plagioclase-quartz veins (Figure 9). Although these felsic veins are not abundant, they provide important paragenetic information allowing us to track the thermal evolution of the system. The distinction between igneous textured plagiogranite segregations and more quartz-rich hydrothermal veins is not readily apparent at the hand specimen scale. These felsic dikelettes and veins cut the diabase at various angles relative to the core axis and range from a few mm to 3 cm thick. The plagioclase in the veins tends to be clear, euhedral to subhedral with well-developed twinning. In contrast, most of the mafic minerals in the veins appear to be inclusions of remnant wall rock augite replaced by hornblende, clinopyroxene, orthopyroxene and biotite. Elongate prismatic grains interpreted to be augite are present in a plagiogranite segregation pod at 4640.32 m (Figure 9e), similar to what was observed in Core 10 (Figure S2d in Supporting Information S1) but are not present in most felsic veins. There is no textural evidence suggesting the

presence of igneous hornblende, however euhedral biotite crystals interpreted as phenocrysts are present in some of the felsic veins. Disseminated fine-grained magnetite is present in some veins. A few small (20–50 µm) euhedral zircon crystals are present in some veins, but do not occur elsewhere in the core samples.

Most of the felsic veins have distinct, but somewhat diffuse borders (Figures 9c, 9e, and 9f), whereas others have sharply defined edges (Figures 9a, 9b, and 9d). Plagioclase phenocrysts can be traced extending from the wall rock into the vein. In these cases, the plagioclase in the diabase is cloudy and filled with inclusions, whereas the portions of the plagioclase crystal in the vein are clear, similar to plagioclase in the vein interior. The dusty appearance of the plagioclase phenocrysts in the wall rock abruptly disappears at the vein boundary, coincident with a change to more Na-rich compositions.

The ratio of quartz to plagioclase is variable with some veins, or portions of veins, similar in appearance to the plagiogranite segregations first seen in Core 10 (Figure S2d in Supporting Information S1 and Figure 9e). Many of the veins examined in thin section are clearly composite veins where earlier plagiogranite segregations were subsequently invaded by quartz-rich hydrothermal veins (Figures 9a, 9b, and 9c).

Only one mineralized open-fracture vein was recovered during the coring of Dike 2 at a depth of 4637.80 m (Figure S11a in Supporting Information S1). The fracture forms one border of a 2 cm quartz-plagioclase-potassium feldspar vein with minor biotite (Figures 9c and 9d), which is the only observed occurrence of K-feldspar in the IDDP-2 core. The fracture surface is coated with euhedral crystals of biotite (Figure S11b in Supporting Information S1) that are overgrown by doubly terminated euhedral quartz crystals (Figure S11c in Supporting Information S1) (Bali et al., 2020; Friðleifsson, Elders, et al., 2020; Zierenberg et al., 2017). This fracture occurred at a temperature near the brittle-ductile transition for basalt and existed long enough for considerable mineralization to form in open space. This is the latest paragenetic stage of mineralization observed in the recovered core and is discussed in more detail below, as the P-T conditions of its formation are most likely those existing in the rocks today.

3.3.6. Mineral Chemistry

Few remnants of olivine phenocrysts from Dike 1 remain, but they are significantly more Fe-rich (Mg# 58–64) than olivine in equilibrium with tholeiitic basalt (Mg# 80–90) (Table S6 in Supporting Information S1). Orthopyroxene that replaces and overgrows olivine is more Mg-rich than orthopyroxene intergrown with hornblende and clinopyroxene that replaces igneous augite (Figure S12a in Supporting Information S1). The only occurrence of igneous orthopyroxene is the large xenocryst present in Dike 2 (Figure S8e in Supporting Information S1), which has higher Mg and lower Ca compared to hydrothermal orthopyroxene (Figure S12b in Supporting Information S1). Hydrothermal orthopyroxene has intermediate Mg-Fe content. There is no systematic difference in opx composition with depth in the core, nor is recrystallized granoblastic textured opx distinguishable from finer grained occurrences.

Hydrothermal clinopyroxene generally overlaps the compositional range of igneous augite (Table S3, Figures S5, and S12 in Supporting Information S1) on a pyroxene quadrilateral plot, but extends to higher Ca and Fe compositions. Hydrothermal clinopyroxene also generally has lower TiO_2, Al_2O_3, Na_2O, and higher MnO than igneous augite (Table S3 in Supporting Information S1).

Amphiboles from Cores 11–13 are mostly magnesiohornblende with less abundant ferrohornblende and a few analyses that plot as actinolite (Table S4 and Figure S13 in Supporting Information S1) and have distinctly higher IV Al contents relative to amphibole in the Hornblende Zone (Figure 7b). Cummingtonite was identified in a single sample (4635.11 m, Table S4 in Supporting Information S1). Amphibole in samples with biotite (shallower than ~4651.5 m) has approximately double the K_2O content compared to deeper samples where biotite is not present (0.51 ± 0.16 vs. 0.24 ± 0.08 wt. % K_2O).

Biotites that are interpreted to be phenocrysts in plagiogranite segregations (based on texture) and those in quartz-plagioclase veins overlap in composition but tend to be more iron- and chlorine-rich than biotite replacing augite (Figure 10). Biotite in the alteration rims of replaced olivine has the highest Mg and lowest Cl and TiO_2 (Table S7 in Supporting Information S1).

Touching pairs of magnetite and ilmenite were analyzed and provide data on the temperature and state of equilibrium of the mineral assemblage that contributes to buffering the oxidation state of the system (Table S8 in Supporting Information S1).
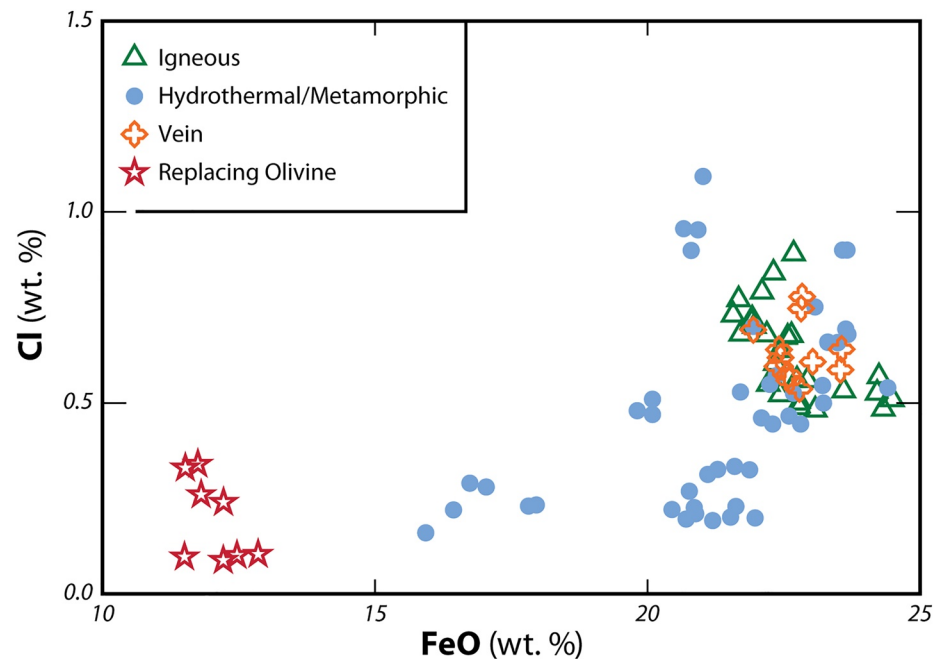
Figure 10. Chlorine versus total iron content (as FeO) of biotite. Euhedral biotites in felsite were interpreted to be igneous based on textural relationships and their compositions largely overlap with biotite in quartz-rich hydrothermal veins and some hydrothermal/metamorphic biotite in the rock matrix. Biotite in the alteration halos of replaced olivine is enriched in MgO relative to hydrothermal biotite.

Feldspar compositions show a wide range that generally corresponds to the paragenetic sequence (Table S2 and Figure S14 in Supporting Information S1). Former igneous plagioclase and plagioclase in the altered rock matrix has average An# of 57.0 (±11.5 one sigma), early amphibole-plagioclase veins average 44.5 (±11.7) and plagioclase in felsite/quartz-plagioclase veins averages 33.2 (±17.1). Plagioclase in Cores 11–13 reverses the trend toward increasing An# with depth observed in the Hornblende Zone (Figure 7a) but has distinctly higher orthoclase content (<0.045 Or, where Or = molar (K/K + Na + Ca)), which correlates to the albite content (Figure 11). Plagioclase in samples with biotite (shallower than ~4651.5 m) has higher K_2O content compared to deeper samples where biotite is not present, and which never exceeds 0.012 Or mole fraction (Figure 11). The only occurrence of potassium feldspar is at 4637.80 m from the quartz-plagioclase vein that borders the only open-space vein recovered.

Quartz was analyzed for Ti concentration, guided by cathode luminescence, to constrain temperature of quartz deposition in relation to paragenetic sequence (Table S9 in Supporting Information S1). The contents of Al_2O_3, K_2O and FeO were also analyzed to screen for the presence of mineral inclusions or contributions from adjacent minerals.

4. Results

4.1. Mineral Geothermometry

Seven independent mineral geothermometers were employed to document the thermal history of the alteration minerals, plagioclase-hornblende, clinopyroxene-orthopyroxene, titanium in amphibole, titanium in quartz, titanium in biotite, plagioclase-Kspar, and magnetite-ilmenite. The geothermometers are discussed in order of their paragenesis from early high temperature alteration to later lower temperature alteration. Important questions we sought to address were (a) What are the temperature ranges recorded as a function of time as constrained by the paragenetic relationships, and (b) What are the present-day temperature and pressure conditions at ~4,500 m in the active geothermal system? The maximum temperature of 426°C measured by logging in January 2017 is clearly a minimum value as the borehole had not then recovered from being cooled by drilling.
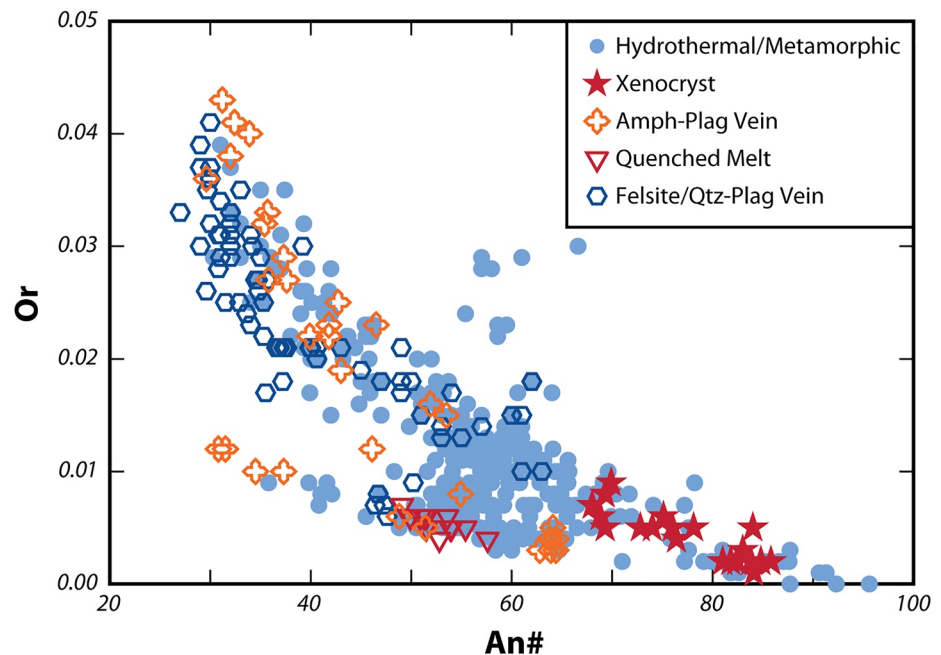
Figure 11. Mole fraction of orthoclase component (Or) plotted against An# for plagioclase in the Pyroxene Zone. Samples from deeper than 4651.5 m do not contain biotite and form a separate trend on the diagram, with Or values ≤0.012.

4.1.1. Plagioclase-Hornblende

Plagioclase and amphibole compositions show compositional variation with depth (Figure 7). Plagioclase in the Geothermal Reservoir Transition Zone (Core 3) has a restricted range with anomalously high An# compared to igneous plagioclase, represented on this plot by the values measured in the least altered diabase sample, a roller assumed to have come from a depth of approximately 4,250 m. An# systematically increases down hole through the Hornblende Zone approaching typical igneous values in the deepest samples, although there is significant scatter and overlap in the data. Weak preservation of igneous zoning patterns and the scatter in An# suggest that plagioclase has not fully equilibrated at a constant temperature. The An# decreases in the Pyroxene Zone with values lower than typical igneous plagioclase. Paragenetically early plagioclase replacing igneous plagioclase is more An-rich than that in cross cutting amphibole-plagioclase veins. Later stage felsite/quartz-plagioclase veins have even lower An# (Figure 7a).

Amphibole compositions change downhole, but there is significant scatter and overlap (Figure 7b). A plot of the mean value of tetrahedral Al, which would be expected to increase with increasing depth/temperature, generally decreases downhole and amphibole from the Pyroxene Zone is invariably more aluminous. Protolith compositions can also influence alteration mineral composition, but there is no apparent systematic change in diabase compositions downhole. The scatter in amphibole compositions and the intergrowth of actinolite and hornblende in the Hornblende Zone suggest that rocks have not fully equilibrated at a constant temperature at any given depth.

Despite the large variability in both plagioclase and amphibole compositions with depth, temperatures calculated from touching (or closely adjacent [tens of μm] mineral pairs that could be expected to touch out of the plane of the thin section) plagioclase-hornblende pairs show a systematic increase of temperatures in the Hornblende and Pyroxene Zones (Figure 12). Temperatures were calculated using the Hora et al. (2013) spreadsheet to implement the edenite-richterite geothermometer of Holland and Blundy (1994). All reported temperatures are for mineral pairs with amphiboles having tetrahedral Al (IV Al) content ≥0.5 per formula unit as actinolite would not be expected to provide equilibrium temperatures.

Plagioclase-amphibole temperatures calculated for Core 3 show a wide range of values from 680° to 910°C, well in excess of estimated temperatures for this depth and well above the depth boiling point curve for
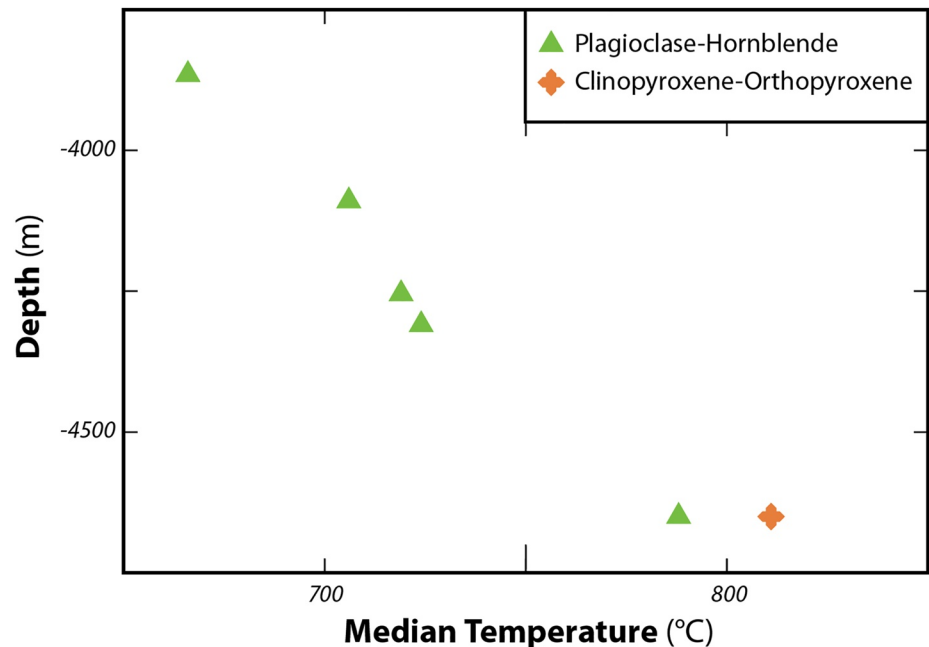
Figure 12. Temperature versus depth plot of median values of calculated plagioclase-hornblende and orthopyroxene-clinopyroxene mineral pairs plotted at the sample recovery depth.

seawater (Figure S15 in Supporting Information S1). We interpret these results not as valid temperatures, but as indications of failure to obtain equilibrium, consistent with the observation of amphibolite facies minerals (calcic plagioclase and hornblende) replacing epidote-actinolite facies minerals (including chlorite).

Plagioclase-hornblende temperatures calculated for the Hornblende Zone show narrower ranges of temperature that generally increase down hole from 686°C (±96°) at 3,865 m to 727°C (±34°) at 4,310 m (Figure S15 in Supporting Information S1). There is considerable scatter in the data, which may be in part related to the approach taken when investigating these samples by electron microprobe, which attempted to capture the maximum variability in mineral compositions as guided by petrography and electron backscatter intensity. We interpret the median values as more representative than the mean values, which are more influenced by outliers. A plot of the median values versus depth (Figure 12) shows a linear increase in temperature with depth ($r^2 = 0.986$) in the Hornblende Zone. The present-day temperature at these depths is presently unconstrained by direct logging, but it is clear that the rocks have cooled since the peak of alteration.

Plagioclase-hornblende temperatures in the Pyroxene Zone give an average value of (785°C ± 39°, $n = 276$), with a distribution skewed to the lower temperature side (Figure 13a). Plagioclase-hornblende pairs in felsite, veins and vein selvages give slightly lower temperatures (728°C ± 17°, $n = 34$). If we assume that the plagioclase-hornblende temperatures record main-stage alteration at approximately the same time at each depth interval, we can calculate a geothermal gradient of 137°C/km ($r^2 = 0.980$), for the cored intervals through the Hornblende Zone to the Pyroxene Zone.

4.1.2. Titanium in Amphibole

Temperatures for amphiboles were calculated using the titanium in amphibole geothermometer (Ernst & Liu, 1998). As discussed below, the assumption that rocks in the Geothermal Reservoir Transition Zone and Hornblende Zone are in equilibrium with a titanium phase is not supported by the magnetite-ilmenite compositions. Rocks from the Pyroxene zone are interpreted to be in equilibrium with ilmenite. Koepke et al. (2008) applied the titanium in amphibole geothermometer to similar hydrothermally altered/metamorphosed sheeted dikes in the ocean crust at IODP Site 1256. McCaig and Harris (2012) also report high temperature (840–1,040°C) amphibole replacing pyroxene in hydrothermally altered diabase and gabbros from dike-gabbro transition at the Atlantis Massif, Mid-Atlantic Ridge, using the Ernst and Liu (1998) geothermometer. Temperatures calculated using the Ti-content in amphibole from IDDP-2 are systematically
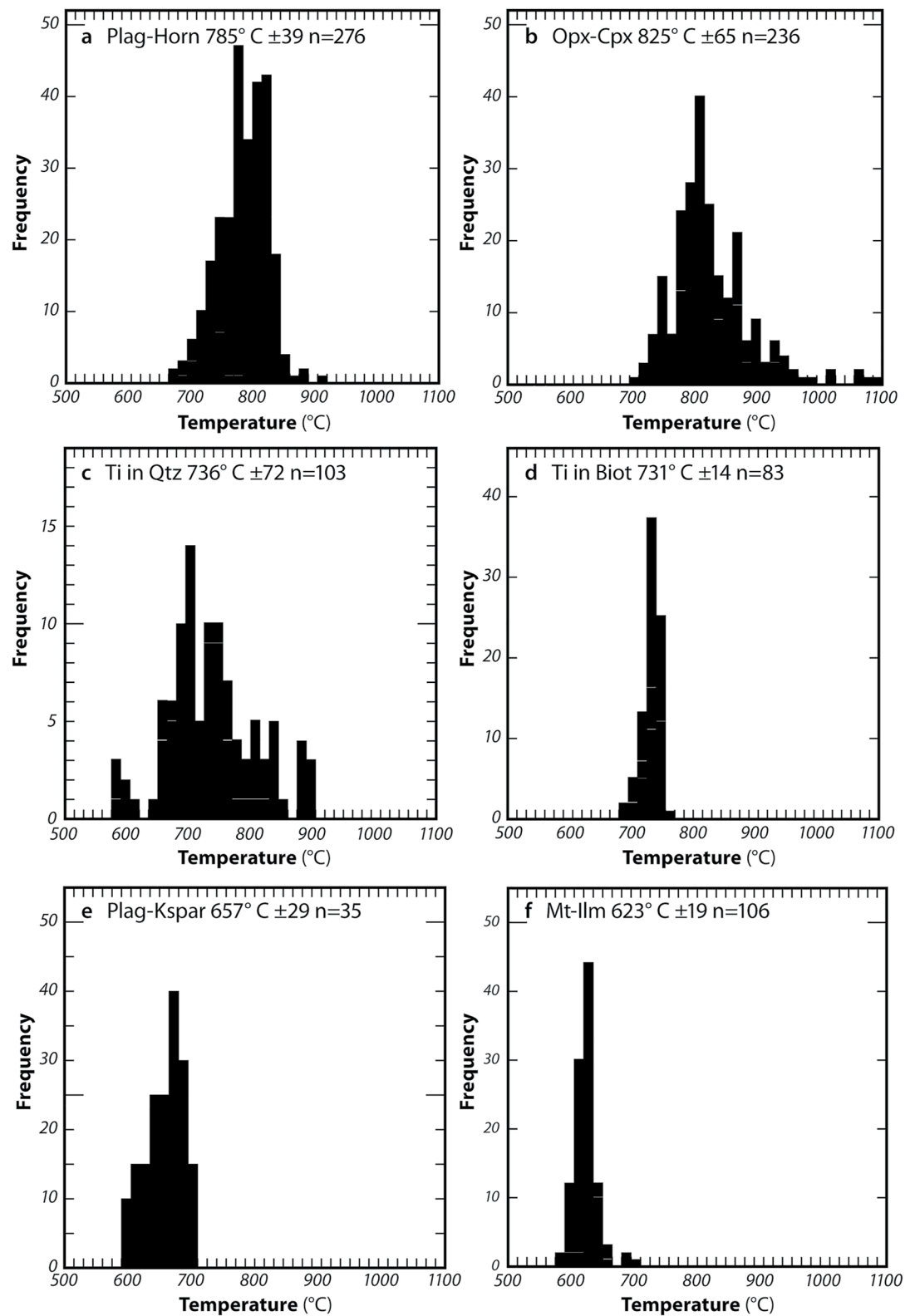
Figure 13. Histograms of mineral geothermometer temperatures calculated for the Pyroxene alteration zone (mean temperature ±1 standard deviation, *n* = number of analyses). (a) Plagioclase-Hornblende. (b) Orthopyroxene-clinopyroxene. (c) Titanium in Quartz. (d) Titanium in Biotite. (e) Plagioclase-K-feldspar. (f) Magnetite-Ilmenite.

lower than plagioclase-hornblende temperatures at the equivalent depth and have average temperatures ranging from 556° to 586°C in the Geothermal Reservoir Transition Zone and Hornblende Zone (Figure S15 in Supporting Information S1). In contrast to the plagioclase-hornblende temperatures, the Ti in amphibole temperatures show no systematic change with depth in the Hornblende Zone (Figure S15 in Supporting Information S1). Amphiboles in the Pyroxene Zone have an average calculated temperature of 704°C (±56, $n = 310$). A plot of plagioclase-hornblende temperatures versus Ti-amphibole temperatures shows no significant correlation ($r^2 = 0.27$; Figure S16 in Supporting Information S1).

4.1.3. Clinopyroxene-Orthopyroxene

The clinopyroxene-orthopyroxene geothermometer of Andersen et al. (1993) was employed to constrain early, high temperature hydrothermal alteration using touching pairs of pyroxene. Temperatures range from near magmatic values down to ~700°C and average 825°C ± 65 ($n-236$) with a distribution that is skewed to higher temperatures (Figure 13b). Some of the highest temperatures are recorded in quenched dike margins or are associated with replaced olivine, reactive areas that are interpreted to form early in the alteration paragenesis. Granoblastic pyroxenes form over the same temperature range as pyroxenes replacing augite. Average pyroxene temperatures are higher than average hornblende-plagioclase temperatures, but the temperature distributions largely overlap with median temperatures near 800°C (Figure 13). Hornblende, clinopyroxene and orthopyroxene are intimately intergrown, however it is reasonable to think that hydrothermal pyroxenes may have ceased forming earlier, and that amphibole continued forming later, as temperatures declined, as indicated in the skewed distributions of temperatures for these two thermometers. It is clear that the main phase of hydrothermal alteration occurred at temperatures well above the commonly assumed brittle-ductile transition temperature for basalts (~600–650°C; Violay et al., 2012, 2015).

4.1.4. Titanium in Quartz

Titanium in quartz temperatures were calculated using the calibration of Huang and Audétat (2012) assuming a pressure of 450 bars (cold hydrostatic recharge) and corrected assuming a TiO_2 activity of 0.53 to reflect equilibrium with ilmenite as the saturated Ti phase, following the approach of Reid et al. (2011). The large range of calculated temperatures is a reflection of both the broad paragenetic stages of quartz deposition and the fact that cathode luminescence was used to target the full extent of Ti variation within a given quartz crystal (Table S9 in Supporting Information S1). Quartz from an early high temperature Plagioclase-Quartz vein gives the highest temperatures, 888°C (±11) (Figure 14a). Small, sparse patches of quartz intergrown with the altered rock matrix average 771°C (±77). Quartz from the quartz-plagioclase eutectic intergrowths from 4655.99 m has an average value of 734°C (±79) (Figure 14b), which is close to the experimentally determined temperature of the water saturated quartz-albite eutectic, 740°C at 2 kbar (Pichavant et al., 1992). Quartz occurs primarily in the felsic segregations and veins, which span the paragenetic history from earlier igneous plagiogranite dikelettes, to the late hydrothermal quartz-rich replacement veins that often overprint the early plagiogranite (Figure 14c). Temperature calculated from Ti in quartz in the felsite/quartz-plagioclase (±biotite) veins averages 710°C (±46°). An effort was made to target the latest stages of quartz formation, including analyzing the rims of euhedral quartz crystals growing into open space in the paragenetically latest stage of mineral growth (Figure 14d). The lowest temperatures that are considered reliable are approximately 585°C. Some quartz has very low titanium, particularly the late-stage polygonal quartz that fill the cavity lined by quenched melt (Figure 14b). We do not interpret these to be valid temperatures, likely due to violation of the underlying assumption that the quartz formed in equilibrium with a titanium mineral, in this case ilmenite. In such cases, the fluid precipitating the quartz was likely no longer in communication with the ilmenite in the rock matrix and the low titanium content results from depletion of dissolved titanium in the fluid, and therefore cannot be interpreted as a reflection of the temperature of quartz precipitation. The temperature of formation of the latest paragenetic stage of quartz growth is one of the criteria used to constrain maximum present-day in situ temperatures, as discussed below.

4.1.5. Titanium in Biotite

The titanium content of biotite can also be used as a geothermometer (Henry et al., 2005). Biotite temperatures show a fairly narrow range (Ave. 731°C, ±14 $n = 83$) with no clear distinction based on occurrence as part of the rock matrix alteration or the presence in felsites and quartz-plagioclase veins. Biotite interpreted to be an igneous phase in felsite, based on petrographic observations, overlaps in temperature with anhedral
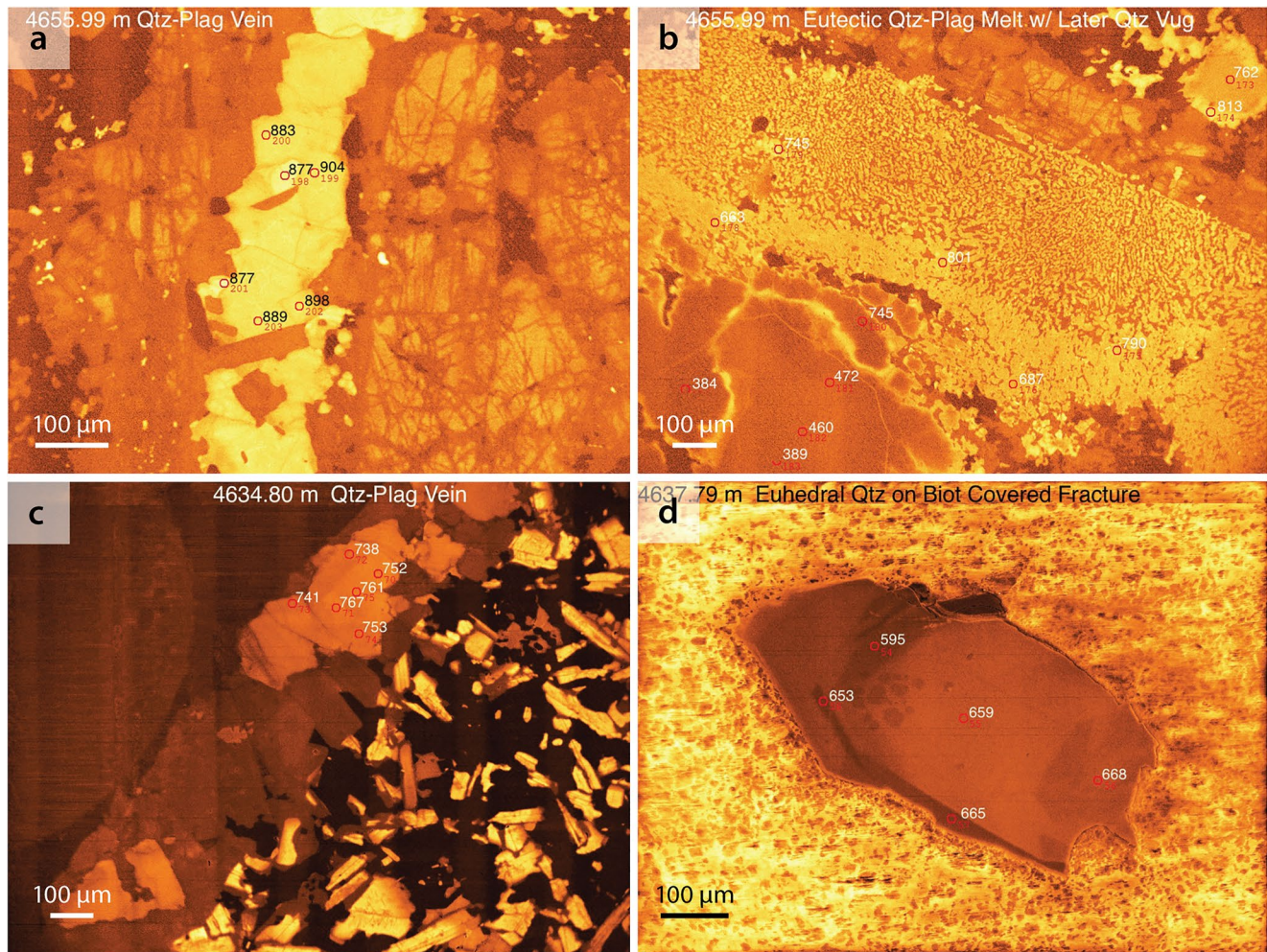
Figure 14. Cathode luminescence images showing calculated Ti in quartz temperatures. (a) Early, high temperature quartz (yellow)—plagioclase (orange) vein cutting altered diabase (4655.99 m). Red circles and numbers are electron microprobe spots, black or white numbers are temperatures (°C) calculated from the Ti content of the quartz. (b) Eutectic intergrowth of quartz-plagioclase quenched from an incipient in situ melt pocket. Crystallization nucleated on an altered plagioclase phenocryst (mottled orange trending diagonally from upper left to middle right). Early high temperature quartz luminesces in various shades of yellow. Late-stage polygonal quartz overgrowing the quenched melt has orange luminescence and low calculated Ti temperatures (<750°C), which are not considered valid as they were not likely in equilibrium with ilmenite. (c) Late-stage quartz (orange)—plagioclase (brown) bounds the left edge of a fragment of altered diabase. Plagioclase in the diabase has yellow to orange luminescence, mafic minerals are dark. (d) Euhedral prismatic quartz crystal separated from the latest-stage open fracture coating and mounted in epoxy (yellow). Quartz nucleated on biotite (not shown) and grew from lower right to upper left.

biotite in hydrothermal quartz-plagioclase veins (Figure 13). Very magnesium-rich biotite that occurs in the alteration halos of replaced olivine phenocrysts in Dike 1 give slightly lower temperatures (682°C, ±14 $n = 8$, Table S7 in Supporting Information S1), which are not included in the histogram shown in Figure 13d as it is not clear that they are part of the main alteration sequence.

4.1.6. Plagioclase-K-Feldspar

Potassium feldspar was seen in only one quartz-plagioclase-K-feldspar vein, which is the wall rock on one side of the latest stage biotite-quartz open-space vein at 4637.79 m. The plagioclase-K-feldspar geothermometer (Putirka, 2008) gives an average temperature of 657°C (±29°) (Figure 13e), with a relatively narrow range of temperatures, consistent with a single paragenetic event.

4.1.7. Magnetite-Ilmenite

Touching pairs of magnetite and ilmenite were analyzed at several depths (Figure 15), including the least altered diabase sample from Core 8 (4250) to near the bottom of the hole (4,656 m), to evaluate the potential as
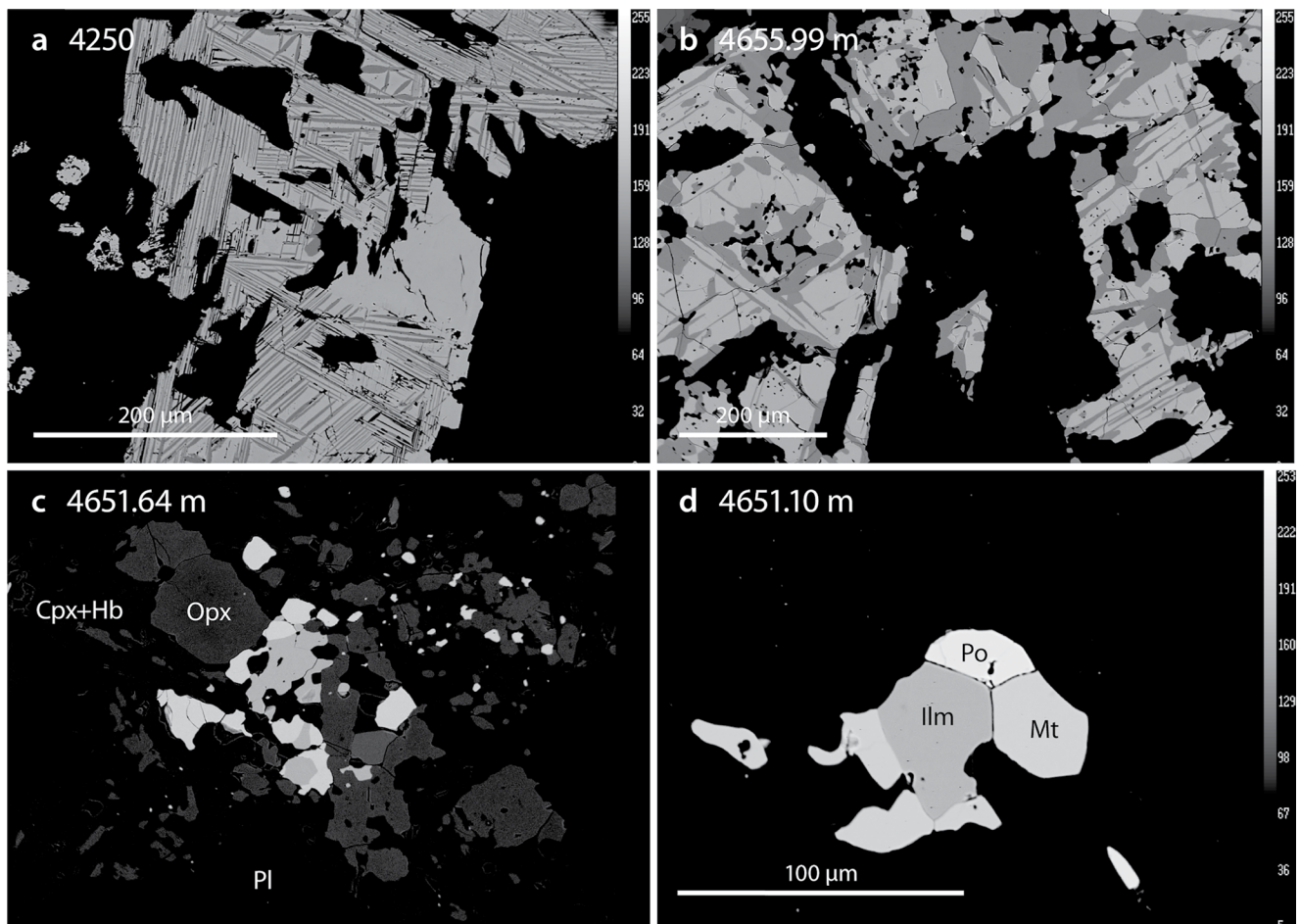
Figure 15. BSE images of magnetite—ilmenite pairs. (a) Typical trellis oxidative exsolution of ilmenite (darker) in igneous titanomagnetite (lighter) in least altered diabase (black, silicates) (4250). (b) Recrystallized rounded blebs of ilmenite in magnetite from the Pyroxene Zone (4655.99 m). (c) Equant intergrown grains of ilmenite (light gray) and magnetite (white) in replaced augite (4651.64 m). (d) Equilibrium triple junction texture of magnetite-ilmenite-pyrrhotite (Po) fO_2−fS_2 buffer assemblage (4651.10 m).

geothermometer (Andersen et al., 1993; Ghiorso & Evans, 2008). Magnetite-ilmenite in contact in oxidative exsolution intergrowths in titanomagnetite from Cores 8 and 10 do not plot on the Mg/Mn equilibrium line of Bacon and Hirschmann (1988) (Figure S17a in Supporting Information S1), and do not produce usable temperature information. In contrast, intergrown Mt-Ilm grains in the Cores 11–13 have grain shapes and grain boundaries indicative of metamorphic equilibrium (Figures 15b–15d), and plot near the equilibrium line. The magnetite-ilmenite temperature histogram shows a narrow range (Figure 13f) with minimum temperatures again of 590–600°C. Calculated oxygen fugacity is 0.58 (±0.2) units below the NiNiO buffer (Figure S17b in Supporting Information S1). While the biotite and two-feldspar temperature ranges are consistent with formation of these minerals over a narrow temperature interval during a single paragenetic stage, magnetite and ilmenite were present throughout the extended alteration history. Magnetite ilmenite pairs typically give lower temperatures relative to silicate geothermometers (e.g., Schiffman et al., 2014) due to the lower closure temperature for the oxides. Our interpretation of the narrow range of temperatures is that magnetite and ilmenite are continuing to exchange Fe-Ti during hydrothermal alteration and cooling, and as such they are more representative of in situ temperatures as opposed to peak alteration temperatures.

4.2. Present Day Temperature

Minimum temperatures for Ti-quartz, plagioclase-K-feldspar and magnetite-ilmenite are all in the 590–600°C range. In an effort to constrain the maximum present-day temperatures, we focused on the latest,

cross cutting paragenetic event, which is a biotite-quartz coated open fracture that formed on the edge of a quartz-plagioclase-K-feldspar vein at 4637.79 m. Cathode luminescence was used to evaluate the growth history of the quartz in these veins (Figure 14d, Table S9 in Supporting Information S1). The latest stage of quartz growth gives the lowest temperature (590–600°C). The convergence of three independent mineral geothermometers at ∼600°C is consistent evidence for the maximum present-day temperature at the bottom of the drill hole. Hand-picked separates of hydrothermal biotite and doubly terminated euhedral quartz were run for oxygen isotope analysis. Because the quartz crystals nucleated on, and overgrew, the biotite, they did not form at the same time, and therefore may not meet the strict requirement for equilibrium growth. None-the-less, they likely formed in close succession from the same, or similar, fluids. The oxygen isotope value obtained on the biotite separate was 3.18‰ (relative to VSMOW); two analyses of quartz gave 6.67‰ and 6.58‰ (Zierenberg et al., 2020). If we assume isotopic equilibrium, we calculate a temperature of 640°C ± 10° using the fractionation equation in Zheng (1993), a value that falls between the Ti in biotite and Ti in quartz temperatures for these samples. The isotopic value of the water from which these minerals precipitated would be ∼4.6‰, consistent with extensive exchange of seawater with basalt at elevated temperature at low water to rock ratio.

Temperature estimates based on mineral geothermometers have subsequently been confirmed by Bali et al. (2020) using analyses of fluid inclusions in quartz from the same samples reported on above from 4637.80 m. These fluid inclusions are either vapor dominant or salt + vapor dominant, consistent with phase separation of seawater at temperatures above the critical curve. Bali et al. (2020) report homogenization temperatures of 600°C ± 20° in both vapor-rich and hypersaline secondary inclusions that represent the last recorded paragenetic event. The salt-rich inclusions contain halite and two yellow K-Fe-Cl minerals along with Cu-Fe sulfide.

Based on the convergence of multiple geothermometers, we propose that the present day in situ temperature at the bottom of the hole is approximately 600°C. While the mineral geothermometers only constrain the maximum temperature at the time of drilling, the presence of olivine and orthopyroxene and the absence of hydrous alteration phases, such as serpentine and brucite, in rocks undergoing active hydrothermal circulation argues that present day temperatures must be greater than ∼550°C (Berman et al., 1986; Day et al., 1985).

4.3. Phase Separation

Seafloor hydrothermal fluids show a large range in salinity due to phase separation of seawater derived fluids in the subsurface (Bischoff & Rosenbauer, 1989; Cowan & Cann, 1988; Kelley & Delaney, 1987; Von Damm & Bischoff, 1988), however Reykjanes fluids have near seawater salinity. As mentioned above, a pressure/temperature log was run in IDDP-2 just prior to coring at the bottom of the hole, and this record confirms that there are feed zones for hydrothermal fluid below 4,500 m (Friðleifsson, Elders, et al., 2020). The log measured temperature of 426°C and pressure of 340 bars at the bottom of the hole, which falls exactly on the two phase curve for a fluid with seawater salinity (Driesner & Heinrich, 2007), consistent with active phase separation of a supercritical fluid of seawater origin at the pressures imposed by the hydrostatic head in the drill hole at the time of the measurement.

For the deeper cores, starting with Core 11, the outside surfaces of the cut core were coated in hematite (Figure 8a). Red hematitic fluid drained from the one open facture at 4637.80 m when the core was extracted from the core barrel. Each successive core showed more extensive hematite staining on exposed surfaces, which is not present in the interior when the core is cut. The mineral assemblage of the core is too reduced to include hematite (Figure S17b in Supporting Information S1). The hematite stain has clearly formed as hot, ferrous-iron-bearing hydrothermal fluid becomes oxidized by mixing with cold oxygenated surface water used as drilling fluid.

Some sections of the core in the interval where biotite is present were observed to be coated by yellow salt that formed on the surfaces of cut core as pore fluid evaporated when the core dried (Figure 8c; Zierenberg et al., 2017). Analysis of this salt by energy dispersive spectrometry in an electron microprobe showed that it is predominantly composed of K-Fe-Cl, some accompanied by Cu, Zn, and Mn, and halite. Two distinct K-Fe-Cl minerals have subsequently been described as daughter minerals in fluid inclusions in terminated

pyramidal quartz overgrowing euhedral biotite that coats the vein surface (Bali et al., 2020). Biotite is not expected to form as an alteration mineral in low-K mid-ocean ridge tholeiitic basaltic dikes. The restriction of biotite alteration to the depth interval around a late-stage vein with K-feldspar and biotite is consistent with reaction of the basaltic dikes with a high salinity K-Fe-Cl rich brine formed by condensation from supercritical seawater. Amphibole and plagioclase that formed in the biotite-bearing zone have higher K content than the underlying rocks that do not contain biotite (Figure 11). The presence of biotite and the increased K content of minerals extends below the Dike 2–3 contact and coincides with a drop in natural gamma logs (Mesfin et al., 2020), which is not consistent with a change in primary lithology, but rather implies K metasomatism, consistent with the presence of K-Fe-Cl-rich brine in the pore space of the core. The narrow temperature peak at ~725°C (Figure 13d), calculated using the Ti in biotite geothermometer, is consistent with a sudden, localized appearance of K-rich brine following peak alteration that formed the dominant plagioclase-hornblende-clinopyroxene-orthopyroxene alteration. A pressure drop related to a fracturing event could cause supercritical seawater to phase separate by condensation of a high salinity brine.

4.4. Origin of Plagiogranite and Felsic Veins

IDDP-2 drill core records the first occurrence of crystalline felsic rocks from the Reykjanes Peninsula, although felsic segregation veins have been observed in thick lava flows (Martin & Sigmarsson, 2005). Leucocratic bands in diabase from Core 5 contain symplectic intergrowths of quartz – oligoclase and are clearly igneous in origin due to late crystallization of residual melt. The first true felsic segregation, dominated by andesine and quartz, was recovered in Core 10 (4309.97 m). The texture of this felsic material, along with the compositional trends (Figure 5) and dacitic composition, are consistent with its formation as a late stage differentiated melt (e.g., Helz & Thornber, 1987; Marsh, 2002; Wanless, et al., 2010). A plagiogranite segregation with diffuse gradational boundaries with the wall rock (4640.32 m) presumably has a similar origin. However, most felsic veins are too quartz-rich to have formed directly by simple crystal fractionation from the host diabase dikes.

The distinction between plagiogranite segregations and more quartz-rich composite and hydrothermal veins is well illustrated by the few samples that were separated for chemical analysis. Two quartz-plagioclase vein samples were large enough to be sampled for whole rock analysis (4635.11 and 4637.80 m; Figure 3). The vein material is silica rich (up to 79% SiO_2) and does not plot along the differentiation trends defined by the diabases and the felsite (dacite). More importantly, the REE concentrations and patterns of the veins are distinctly different. REE are significantly depleted relative to the felsite and the chondrite normalized REE patterns (Figure 5g) have wing-like enrichments in light and heavy REE and strongly developed positive europium anomalies. The pattern is similar to that of seafloor hydrothermal fluids and geothermal fluid produced from the Reykjanes reservoir (Fowler et al., 2019). Similar patterns are seen in epidote from hydrothermal veins in the Reykjanes reservoir (Fowler & Zierenberg, 2015).

Silica-rich plagiogranite veins and segregations are well known from oceanic crust and ophiolites and multiple processes have been proposed for their origin. Many studies (e.g., Koepke et al., 2007), have emphasized the role of hydrous melting of basaltic/gabbroic rocks as a source of felsic magmas. Many Icelandic rhyolites have formed by partial melting of hydrothermally altered basalt (Jónasson, 2007), and the IDDP-1 hole drilled at the Krafla geothermal field in North Iceland drilled into rhyolite magma formed by this process (Elders et al., 2011; Zierenberg et al., 2013). What role does partial melting play in the generation of the felsic veins recovered in the deep core at Reykjanes?

The only evidence observed for in situ melting of the recovered rocks is the small pocket of quartz-An_{50} eutectic intergrowth at 4655.99 m, which we interpret as a quenched incipient melt (Figures S9e and S10 in Supporting Information S1). The melt formed after initial hydrothermal alteration of the rock and quench crystals nucleated on altered plagioclase crystals and hornblende altered augite. Melting initiated as the rocks were being cooled (retrograde melting) by hydrothermal circulation due to lowering of the melting temperature due to increased activity of water. The composition of the melt estimated by EMP is compared to the bulk rock composition data on Figure 16. The composition of the Krafla rhyolite magma encountered in IDDP-1, which formed by partial melting of hydrothermally altered basalt is included for comparison (Zierenberg et al., 2013). The in situ melt is very high in silica with low concentrations of Mg, Fe, and TiO_2 (Figures16a–16c) that fall on a roughly linear trend with the other felsic rocks, including the Krafla rhyolite.
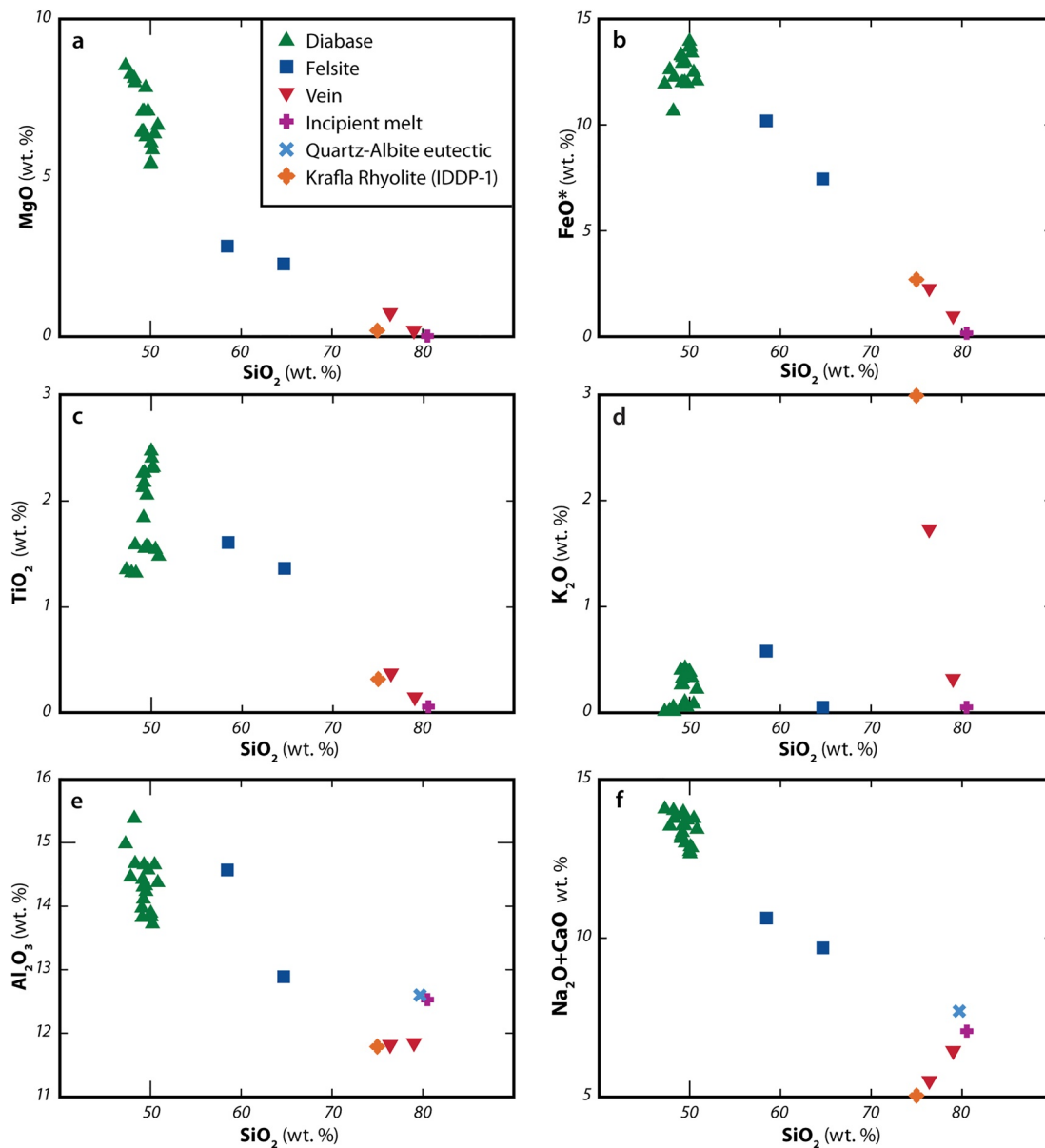
Figure 16. Compositional trends plotted relative to silica content. (a) MgO versus SiO_2. (b) FeO versus SiO_2. (c) TiO_2 versus SiO_2. (d) K_2O versus SiO_2. (e) Al_2O_3 versus SiO_2. (f) ($Na_2O + CaO$) versus SiO_2. The Krafla rhyolite magma drilled by IDDP-1 (Zierenberg et al., 2013) and the composition of the albite-quartz eutectic (Pichavant et al., 1992) are shown for comparison.

The incipient melt also has very low K_2O, which distinguishes it from the Krafla rhyolite and the one felsic vein sample from Reykjanes that contains K feldspar. The Krafla rhyolite was proposed to have been derived by partial melting of hydrothermally altered basalts containing hornblende as the primary hydrous phase (Zierenberg et al., 2013), whereas there is no textural evidence of amphibole melting in the rocks recovered at Reykjanes. The elevated K_2O content in the felsic vein sample from Reykjanes points to the involvement of the K-Fe-Cl rich brine, or rocks that have interacted with such a brine. The in situ incipient melt is present in diabase below the biotite bearing zone. The temperature of crystallization (734°C) calculated using Ti-in-quartz, the silica-aluminum ratio, and the sum of major cations (Na + Ca) are a close match for the quartz-albite eutectic temperature (740°) determined by Pichavant et al. (1992) and is consistent with plagioclase melting induced by interaction with a silica-bearing aqueous fluid.

Melt from nearby hydrothermally altered sheeted dikes could have migrated through the rocks cored. Lundstrom (2020) presents experimental work showing that hydrous quartz-albite melts exist continuously from magmatic-like conditions at >800°C down to 330°C, where conditions would be described as clearly hydrothermal. Many of the felsic veins have earlier igneous-appearing textures that are overprinted with later, more quartz-rich sugary textures, but there are no cross-cutting relationships suggesting separate phases of veining. The vein textures and the REE patterns are consistent with an evolution from magmatic melts to melts with a high water content that would be described as hydrothermal with no boundary separating the end members, as proposed by Lundstrom (2020). The REE patterns clearly distinguish between the magmatic endmember of the plagiogranites and the hydrothermal endmember of the felsic veins, but more work is needed to try to address if there are abrupt or transitional changes, especially in composite veins. Attempting to distinguish between magmatic dikelettes and hydrothermal veins in the cores available may not be a useful pursuit. Low viscosity felsic melts were able to find permeable pathways through the diabases and formed dacitic veins with igneous textures. In some cases, more evolved water-rich fluids could continue to exploit these same permeable pathways forming more silica-rich veins which share textural and compositional, particularly REE, similarities to hydrothermal veins. The evidence at hand supports a local, as opposed to a deeper perhaps gabbroic, source for the felsites and veins.

4.5. Discussion of Alteration Zones

4.5.1. Geothermal Reservoir Transition Zone

The Geothermal Reservoir Transition Zone is the only zone that shows clear evidence of a prograde alteration sequence, i.e., higher temperature alteration phases (calcic plagioclase, hornblende) are replacing earlier formed minerals of the epidote-actinolite facies (plus chlorite, albite and titanite) that characterize the geothermal reservoir that is presently supporting power production at Reykjanes. The concept of a more permeable hydrothermal reservoir with a storage capacity overlain by a lower permeability cap rock zone is well established in the geothermal industry and is the basis for quantitative assessment of geothermal resources (Glassley, 2010). One of the most important results of the IDDP-2 drilling was that it showed the producible geothermal reservoir extends from the currently exploited depths of 2–2.5 km to approximately 3.5 km. This nearly doubles the size of the potentially exploitable geothermal resource (Friðleifsson, Pálsson, et al., 2020). Previous work had clearly established the location of the hydrothermal up flow chimney feeding the Reykjanes reservoir (Friðleifsson, Elders, et al., 2020) and there was no doubt that drilling into this zone would encounter high temperature, but an economically viable resource also requires sufficient permeability to produce fluids at a rate that will support energy production.

At the time of this writing, after many months of fluid injection to stimulate permeability, the IDDP-2 well was allowed to heat toward thermal equilibrium. However, the well has not been produced due to technical issues with the integrity of the well casing and precipitation of scale minerals blocking flow up the well, which has also precluded downhole logging or fluid sampling. Because of this, the temperature, fluid composition and productivity of this well cannot to be quantified. None-the-less, the discovery of a major fluid loss zone at around 3.4 km depth represents a significant discovery in terms of the potential for production of high enthalpy fluids for energy production. Unfortunately, this major loss zone also precluded return of drilling fluids and rock cuttings to the surface during drilling, severely limiting our knowledge of the down hole geology below the loss circulation zone.

Rock similar to the drill core recovered in Core 3 has been described in previous studies based on cuttings from other Reykjanes deep drill holes (Marks et al., 2011; Marks, Schiffman, Zierenberg, Elders, et al., 2010; Marks, Schiffman, Zierenberg, Franzson, & Friðleifsson, 2010). Limited coring in deep drill holes (Figure 1) provided important context for the temporal evolution of alteration events in the deeper parts of the currently exploited Reykjanes reservoir (Fowler & Zierenberg, 2016; Fowler et al., 2015). These previous studies documented the presence of alteration minerals of the amphibole facies partially replacing minerals of the epidote-actinolite facies. One distinguishing characteristic of this prograde alteration is the presence of hydrothermal anorthite and calcic diopside-hedenbergite. The anorthite and diopside-hedenbergite in Core 3 are distinctly more calcium rich than the precursor igneous plagioclase and augite. Is this because (a) the host rock was more calcic, (b) these rocks have undergone calcium metasomatism, or (c) is it a function of the hydrothermal mineral assemblage?

The diabase samples recovered from Core 3 are compositionally distinct from all the deeper diabase dikes. They are the least evolved in terms of incompatible elements and they have the highest calcium contents. Quantification of element gains and losses in hydrothermally altered rocks is difficult without clear knowledge of the composition of unaltered precursors. The calcium content falls along expected fractionation trends versus zirconium (Figure 5c), but the rocks appear to have lost some sodium (Figure 5d) and potassium (Figure 5e). Based on relatively immobile elements, particularly REE (Figure 5g) and Nb, Zr, and Y (Figure 5h), these rocks are clearly transitional between the TEE and TED suites defined by Gee et al. (1998). Despite the differences in protolith composition, the presence of highly calcic hydrothermal plagioclase and clinopyroxene appears to be related to mineral reactions, not protolith composition or metasomatic addition of calcium.

Focusing on the calcic nature of hydrothermal plagioclase and clinopyroxene is perhaps misguided as calcium is relatively soluble and easily mobilized in hydrothermal fluids. Prograde hydrothermal alteration of basalt in Icelandic geothermal systems proceeds from zeolite facies to smectite, mixed-layered clay, chlorite, chlorite-epidote, and epidote-actinolite facies before reaching amphibolite facies (Franzson et al., 2002; Kristmannsdóttir, 1979; Marks, Schiffman, Zierenberg, Elders, et al., 2010; Marks, Schiffman, Zierenberg, Franzson, & Friðleifsson, 2010). The change to higher temperature amphibolite facies alteration is marked by the appearance of calcic plagioclase and hornblende, both relatively aluminous minerals. Ironically, the formation of hydrothermal anorthite may be dependent on albitization. Basalts undergoing progressive alteration remain little recrystallized until igneous plagioclase becomes albitized. Na-plagioclase is much less aluminous than igneous plagioclase. It is the release of relatively immobile aluminum that allows to the rock to recrystallize to minerals like chlorite, epidote and actinolite that have high Al/Si ratios marking the onset of greenschist facies mineral formation and extensive recrystallization of the basalt.

The transition to amphibole facies is marked by the breakdown of aluminous chlorite and epidote freeing aluminum to form anorthite and hornblende. Rocks deeper than ~2 km in the Reykjanes system record the initiation of this replacement reaction in response to higher temperature (Marks, Schiffman, Zierenberg, Elders, et al., 2010; Marks, Schiffman, Zierenberg, Franzson, & Friðleifsson, 2010). The core recovered at 3,648 m in IDDP-2 shows that the rocks at that depth have not equilibrated to the local temperature and suggest that hydrothermal alteration is ongoing and is, therefore, still part of the Geothermal Reservoir Transition Zone. This may have implications for the interpretation of sea floor hydrothermal fluids, as discussed later in this paper.

4.5.2. Hornblende Zone

The lack of drill cuttings returned to the rig floor and the limited availability of drill core preclude determining the depth range of the Hornblende Zone. This zone is characterized by excellent preservation of igneous texture despite pervasive alteration, with near complete alteration of igneous plagioclase and replacement of augite by hornblende. The range of plagioclase and amphibole compositions and the presence of intergrown actinolite and hornblende indicate that the rocks in the Hornblende Zone have not fully equilibrated, consistent with evidence from the oxide minerals. Petrographic evidence for earlier, lower temperature alteration in these rocks is lacking, nor is there any evidence of retrograde alteration. The recovered cores appear to show a single phase of alteration at a medium temperature of 679°C at 3,865 m to 731°C at 4,310 m. It is not clear if the dikes were emplaced into an active hydrothermal system at these temperatures or if a rapidly evolving hydrothermal system developed with no significant preservation lower temperature alteration. The temperatures of the peak alteration are also likely a few hundred degrees higher than the present-day temperature, but we do not observe evidence of continued alteration during cooling.

One surprising feature of these rocks is the pervasive nature of the alteration given the low intrinsic permeability (Gibert et al., 2020) and the near absence of veining in the majority of the core samples recovered. Approximately 3 m of continuous core was recovered in Core 5 with only a few, mm scale veins completely filled by hornblende (Figure 6), yet there are essentially no primary igneous phases remaining. The rocks are pervasively altered but show little evidence for compositional change other than addition of water to form hornblende. At the temperatures recorded for alteration the hydrothermal fluid (evolved seawater) would have been well into the single-phase supercritical field with vapor-like properties. Clearly this low density, low viscosity vapor-like fluid was able to completely penetrate the rock altering the plagioclase to intermediate compositions and hydrating the pyroxene to form hornblende. The formation of hornblende

from augite requires addition of aluminum, sodium and potassium, which could be remobilized from plagioclase, but there is no clear loss or gain of elements recorded by the bulk composition of these rocks.

Given that few cores were recovered, we did not sample the permeable pathways that are likely present in between the cored intervals. The lack of clear evidence for fluid flow paths may therefore not be a robust observation, however no feed zones were detected by downhole temperature logging in the Hornblende Zone. The one exception was the very limited and fragmented core recovered in Core 8. Some of the core fragments were intensely veined with several overlapping generations of quartz-plagioclase ± amphibole replacement veins with minor amounts of shearing and fragmentation. Core 8 consists of very fine-grained diabase with some chilled margin preserved. It is well established that permeability in the deeper, intrusive-dominated portions of the Icelandic geothermal fields is often associated with dike margins (Palgan et al., 2020). The limited material available from Core 8 appears to represent a prior potential feed zone that focused fluid flow along a dike margin, and it therefore may warrant more detailed study. One open question is "Were hypersaline fluids, similar to those documented from the underlying Pyroxene Zone, able to penetrate into the shallower portions of the geothermal system?" Fluid inclusions in the vein material may provide an answer. We note that Core 8 and Core 10 both contain trace amounts of biotite. Some plagioclase in Core 8 also contains high concentrations of iron (Table S2 in Supporting Information S1). In the following section we relate the formation of biotite in the upper portion of the Pyroxene Zone to the localized presence of a K-Fe-rich hypersaline brine formed by brine condensation from supercritical evolved seawater.

4.5.3. Pyroxene Zone

The recovery of a nearly continuous section of core in the Pyroxene Zone records the transition from magmatic to hydrothermal environments that, coupled with data from six independent geothermometers, fluid inclusions (Bali et al., 2020), and stable isotopes (Zierenberg et al., 2020), provides a detailed picture of the temperature-time events that have affected the rocks. While temperature can be quantified, only the relative time sequence can be inferred from the paragenetic sequence. The highest temperatures are recorded by the two pyroxene geothermometer and they extend to near magmatic temperatures. The highest temperatures are recorded in what would be expected to be the most reactive phases, replaced olivine and the fine-grained quenched margins of dikes. Initial alteration of olivine to orthopyroxene is an indication of increased silica activity due to the penetration of a fluid phase transporting silica into the rocks at temperatures in excess of 1,000°C. Olivine and orthopyroxene are not in equilibrium (evidenced by the one-way alteration path) and the composition of the olivine shifted to iron-rich compositions that are not compatible with the magnesium-rich orthopyroxene that initially replaces them. However, high temperatures are recorded by cpx-opx (+hornblende) in the alteration coronas and pseudomorphs of replaced olivine. Temperatures above 1,000°C are also preserved in intergrown cpx-opx (+hornblende) in chilled margins, clearly indicating that fluids are interacting with very hot rock. At these temperatures, the seawater would have separated into a low-density vapor plus halite. The main phase of alteration of the rock to the plagioclase-hornblende-clinopyroxene-orthopyroxene assemblage occurred at approximately 800° as recorded by both the plagioclase-amphibole and two pyroxene geothermometers. The pyroxene thermometer shows a skewed distribution to the high temperature side (Figure 13b) and better preserves the initial stages of alteration while the plagioclase-hornblende thermometer continues to record lower temperatures as fluid circulation and cooling progresses (Figure 13a). Quartz-plagioclase replacement veins started to form at temperatures near 900°C (Figure 13c). A localized pocket of incipient melt formed and crystallized along altered wall rock at ~734°C, a clear example of retrograde melting in rock undergoing cooling due to lowering of the solidus due to increase water activity. Felsic patches and veins appear to record a continuous transition from late stage plagiogranite differentiated melts to overprinting quartz-rich plagioclase veins. The average temperature recorded in the felsite/veins by the plagioclase-amphibole geothermometer is 728°C while that recorded by Ti in quartz is 710°C. The average formation temperature of the biotite is 727°C, overlapping with the average temperature of the felsite veins.

The latest event recorded in the recovered core is the open-space fracture at 4637.8 m (Figure S11 in Supporting Information S1) and we use the information from that interval to constrain the present-day temperature of the hydrothermal system. Quartz in the felsite wall rock gives an average temperature of 700°C (±42°). Co-existing plagioclase-K-spar in the felsite give a temperature of 657°C (±29°). The oxygen isotope temperature calculated for biotite and quartz in the open fracture give and equilibrium temperature of

640°C while titanium in quartz from the prismatic crystals averages 657°C (±42). The latest growth rims on prismatic quartz crystals formed at 580°–600°C, based on their titanium content. Co-existing vapor-rich and hypersaline fluid inclusions in healed fractures in these same quartz crystals have homogenization temperatures of 600°C (±20°) (Bali et al., 2020). The lowest temperature recorded in the rocks gives a reliable estimate of the maximum in situ temperatures today in this active hydrothermal system. The complete absence of hydrous alteration in olivine and orthopyroxene suggests the temperatures exceed the upper stability limit of serpentine and talc, ~550°C at these relatively shallow depths (Berman et al., 1986; Day et al., 1985). Seawater-derived hydrothermal fluid is entering the bore hole at depths greater than 4,500 m and is undergoing active phase separation at the pressure induced on the bore hole at the time of measurement, which constrains the temperature to the phase boundary at 427°C and 340 bars (Friðleifsson, Elders, et al., 2020).

4.6. Implications for Seafloor Hydrothermal Systems, Altered Oceanic Crust, and Ophiolites

The main phase of alteration in the Pyroxene Zone took place at ~800°C in the presence of a seawater-derived vapor-like fluid producing the assemblage plagioclase (An_{60})—hornblende—clinopyroxene (Wo_{45} $En_{36}Fs_{19}$)—orthopyroxene (En_{49})—magnetite—ilmenite—apatite—isocubanite with chalcopyrite exsolution ± quartz ± olivine (Fo_{60}) ±pyrrhotite. Locally, rocks reacted with a high salinity brine producing biotite ($Mg\#_{45}$), and in one vein, K-feldspar. We now turn to the questions (a) "Are the mineral phases observed in the IDDP-2 borehole those that constrain the composition of submarine hydrothermal fluids" and (b) "How does this mineral assemblage compare to alteration assemblages observed in the sheeted dike section of oceanic crust and ophiolites?"

Hydrothermal olivine has not been previously reported, to our knowledge, from altered sheeted dikes, but has been reported from ultramafic rocks drilled at IODP Site 735B (Dick et al., 1992). The most extensive studies of alteration of sheeted dikes recovered from intact oceanic crust comes from scientific oceanic drilling at Hole 504B and 1256D (Figure 1). Hydrothermal alteration of the sheeted dike section of the oceanic crust has been investigated in numerous drill holes, as reported in Alt et al. (1996, 2010). The alteration mineral assemblages reported are very similar to those in the Geothermal Reservoir Transition Zone of IDDP-2. In the IODP samples, high temperature (>400°C) hornblende facies alteration is indicated by calcic plagioclase, hornblende and hydrothermal clinopyroxene. The rocks are not as pervasively altered as we report from IDDP-2 and most samples contain epidote, actinolite and albite in addition to the amphibole facies minerals. One significant difference is that the IODP hydrothermally altered dikes show a retrograde alteration sequence with early amphibole facies minerals veined and replaced with lower temperature minerals formed as the hydrothermal system weakened and cooled, which is in contrast to the prograde sequence recorded in the Geothermal Reservoir Transition Zone of IDDP-2 where hornblende is observed overgrowing and replacing actinolite.

Granoblastic dikes recovered at the sheeted dike-gabbro transition at IODP Site 1256 (Koepke et al., 2008) have the same mineral assemblage as the rocks from the Pyroxene Zone in IDDP-2. At Site 1256, the recrystallized dikes formed in response to thermal (contact) metamorphism driven by gabbro intrusions, followed by hydrothermal alteration. Granoblastic textured rocks formed by high temperature contact metamorphism related to dike emplacement have been previously described in dill cuttings from the drill holes in the deepest part of the Reykjanes geothermal reservoir at depths of ~2,200–2,700 m (Marks et al., 2011). Granoblastic textured zones are rare in the rocks recovered from the deepest section of IDDP-2 where they occur intergrown with altered rocks retaining their igneous texture and appear as part of the high temperature hydrothermal alteration. Contact metamorphism may be expected in wall rocks near quenched dike margins, but no evidence for this is recorded in the rocks and the granoblastic textured zones occur in dike interiors away from chilled margins. Koepke et al. (2008) describe an earlier, higher temperature, dry paragenesis for the granoblastic clinopyroxene-orthopyroxene-plagioclase-magnetite-ilmenite assemblage, followed by a lower temperature, wet paragenesis amph-cpx-pl-mt-ilm assemblage formed in response to fluids derived from the gabbros. In contrast, hornblende is intimately intergrown with cpx and opx in the IDDP-2 rocks and the granoblastic textured rocks formed at the same paragenetic stage and temperatures as the main stage hydrothermal alteration.

Granoblastic textured rocks with mineral assemblages similar to those observed in the Pyroxene Zone in IDDP-2 have also been reported from Hess and Pito Deeps in the Pacific and the Cyprus and Oman

ophiolites (Gillis, 2008; Gillis & Roberts, 1999). The mineralogy, mineral chemistry, paragenetic relationships, and geothermometry of hornblende- and pyroxene-hornfels that record the magma-hydrothermal transition in the Troodos Ophiolite, Cyprus, are nearly identical to what we observe in the deep drill cores from IDDP-2 (Gillis & Roberts, 1999). The hornfels alteration occurs at the top of gabbroic bodies that intrude the base of the sheeted dikes and is associated with plagiogranite segregations and veins. The setting is similar to that drilled in IODP Hole 1256, and in both cases hornfels is interpreted to form during prograde metamorphism of hydrothermally altered dikes near the dike-gabbro transition. These occurrences are from fast and intermediate rate spreading centers where shallow, persistent axial magma chambers are thought to be common at the base of sheeted dike complexes. In these setting, hydrothermally altered diabase may be subject to repeated episodes of prograde, contact metamorphism during intrusion of new gabbroic bodies. The Reykjanes Ridge is a slow spreading ridge with an anonymously thick crustal section due to excess melting related to the Iceland Hot Spot. While the extent of sheeted dikes below the bottom of the drill hole at 4.5 km is not known, there is no indication from geophysical surveys that suggest the presence of shallow melt bodies under the Reykjanes Peninsula (Blanck et al., 2020; Martins, et al., 2020).

A key difference between all of the examples of high temperature pyroxene facies mineral assemblages described from the oceanic crust and ophiolites compared to the IDDP-2 rocks is that the IDDP-2 hole is the only one drilled into an active geothermal system. There is no evidence for prograde, contact metamorphism at Reykjanes and all of the alteration has occurred in an active hydrothermal system that has cooled approximately 200°C since the main stage of high temperature alteration. The rocks recovered from IDDP-2 were quenched during drilling from in situ temperatures of approximately 600°C, and there is no overprinting alteration or deformation related to off-axis hydrothermal circulation tectonism, or emplacement, as occurs in the case of the ophiolites. More importantly, the IDDP-2 deep alteration is the only high temperature reaction zone where we can demonstrate the presence of a hydrothermal up-flow zone. This allows a direct comparison of the Reykjanes geothermal fluid to mid-ocean ridge vent fluids, which overlap in composition.

Numerous studies have used either seafloor hydrothermal fluid compositions or the compositions of fluids from laboratory experiments to infer the mineral assemblages in the high temperature reaction zone that is assumed to control fluid composition. Recent reviews of these studies include Seyfried and Shanks (2004), German and Seyfried (2014), Humphris and Klein (2018), and Schwarzenbach and Steele-MacInnis (2020). There is general agreement that the high temperature reaction zone is located near the base of the sheeted dike section at a depth of ~4.5 km below the sea level. Phase separation plays a critical role in many seafloor hydrothermal systems with estimates of subseafloor temperatures in the 400°–500°C range. These temperatures are lower than the present-day temperatures at 4.5 km under the Reykjanes system and at least 300°C lower than the conditions present during the main-stage alteration of the sheet dikes recovered at the base of IDDP-2. None of these papers suggest control of the fluid compositions by the mineral assemblage documented in the Pyroxene Zone at Reykjanes. Rather, there is general agreement that the fluid compositions are set by reaction with basaltic rocks with greenschist facies alteration minerals including chlorite, amphibole, albite and epidote. In the IDDP-2 samples, chlorite, albite and epidote are last observed in the Geothermal Reservoir Transition Zone and are not observed deeper than 3,865 m. These greenschist facies minerals are no longer stable in the transition zone where they are being replaced by the calcic plagioclase and hornblende that characterize the Hornblende Zone.

Epidosites have been widely recognized as zones recording extensive alteration by reaction with hydrothermal fluids related to black smoker systems (Richardson et al., 1987; Schiffman et al., 1987) and continue to be referenced as the source rocks for seafloor hydrothermal fluids that form massive sulfide deposits as the 'Epidosites contain virtually no sulfide and are highly depleted in Cu, Zn, and other metals' (Schwarzenbach & Steele-MacInnis, 2020). Schiffman and Smith (1988) and Seyfried et al. (1988) clearly establish that epidosites are produced by extensive reaction of basaltic dikes at high water-rock ratios which depletes the rock in soluble elements including boron, alkali metals and base metals. Alteration in these upflow zones creates permeable pathways due to mineral dissolution that focusses further hydrothermal upflow (Cann et al., 2015). A consequence of the extensive alteration at high water-rock ratio is that these rocks can no longer supply metals and soluble elements, including boron and alkali metals, to the hydrothermal fluids.

In contrast, black smoker fluids are metal-rich and the concentration of soluble elements in seafloor hydrothermal fluids requires the fluid to continually react with relatively fresh basalt at low water to rock ratios (Seyfried et al., 1988; Von Damm et al., 1985). While epidosites are clearly not formed in the deep high temperature reaction zone and do not control the composition of black smoker fluids, they do provide important evidence that hydrothermal fluids continue to interact with basalts in focused fluid upflow zones where high time-integrated water to rock ratios are possible (Cann et al., 2015; Gilgen et al., 2016).

An implicit, but rarely stated, assumption is that fluids generated in submarine high temperature reaction zones raise rapidly to the seafloor with minimal interaction with rocks along their path through their up-flow zone. Short lived radiogenic isotope concentrations in submarine hydrothermal fluid (Kadko & Butterfield, 1998) and the Reykjanes geothermal fluid (Kadko et al., 2007) have been interpreted to reflect very short residence times (1–4 years) in the subsurface from the onset of high temperature hydrothermal alteration, supporting rapid upflow of hydrothermal fluid. Based on thermal and fluid flow constraints, Coogan (2008) argues that temperatures exceed greenschist facies at the base of the sheeted dikes and that the dikes are interacting with hot fluids in the up-flow zone underlying seafloor vents. These arguments are presented in the context of medium- to fast-spreading oceanic crust where heat transfer is mediated by the conductive boundary layer of an axial magma chamber cooled by hydrothermal convection. Many have argued that sustained high temperature venting can only be supported by magmatic activity (Lister, 1974; Lowell & Germanovich, 2004) with conductive heat flow across a thin (tens of m) conductive boundary layer. Jupp and Schultz (2000, 2004) explore the relationship between permeability-controlled fluid flow and thermal conduction as a constraint on the maximum temperature of hydrothermal vents driven by basaltic melt. Sustained hydrothermal upflow of high temperature (350°–400°C) fluid is only possible at relatively low permeabilities in the range of $\sim 5 \times 10^{-14}$ m^2 (Coumou et al., 2008, 2009; Geiger et al., 2006; Ingebritsen et al., 2010). The near absence of open fractures in the IDDP-2 core and the petrographic observations detailed in this study confirm that the recovered rocks have been pervasively altered despite the lack of intrinsic permeability, consistent with the modeling of seafloor hydrothermal systems (Scott et al., 2017). Shallow magma lenses that typically underlie medium to fast spreading mid-ocean ridges are clearly sufficient to drive sustained high temperature hydrothermal discharge, but are they necessary?

Reykjanes is a slow spreading rift (1.8 cm/yr; Sigmundsson et al., 2020). Wilcock and Delaney (1996) suggest that long-lived, high temperature geothermal circulation at slow spreading ridges can be maintained by progressive downward migration of a thermal cracking front in crystalline rock. Emplacement of magma in slow spreading environments is episodic with intervening periods of amagmatic tectonic extension that can create permeable pathways for deep circulation of seawater (Cannat, 1993; McCaig & Harris, 2012). Basalts erupted on the Reykjanes peninsula derive from fissure feed eruptions with a deep source that does not indicate storage in a shallow magma reservoir (Arnórsson, 1995).

The Reykjanes geothermal system is thought to have been active since at least the last glacial maximum (Fowler et al., 2015; Franzson et al., 2002; Hardardóttir et al., 2009) with a minimum thermal output of 130 MW (Fridriksson et al., 2006). No data have been presented to suggest that the Reykjanes system has not been continuously active, and deep hydrothermal alteration in the Hornblende and Pyroxene Zones described in this paper shows only retrograde cooling with no overprinting suggestive of episodic activity. In contrast to the observations presented in Coogan (2008) that high temperature, pyroxene-bearing alteration at the base of sheeted dikes in medium to fast spreading environments is localized in heterogeneous alteration zones, the alteration at Reykjanes is homogeneous and pervasive. Coogan (2008) correctly points out that none of the known high temperature alteration assemblages in oceanic crust or ophiolites can be traced to focused up-flow zones that supported near surface hydrothermal discharge, whereas the IDDP-2 drill hole was targeted to penetrate the hydrothermal up-flow chimney that feeds the Reykjanes geothermal system. While we cannot eliminate the possibility that the Reykjanes system is underlain and thermally driven by an active basaltic melt lens, there is no evidence for any shallow magma bodies below the Reykjanes geothermal field despite extensive geophysical surveys conducted in the area (Blanck et al., 2020; Martins, et al., 2020).

High-temperature, off-axis-hydrothermal vents have been located on several slow to intermediate rate spreading centers (Clague et al., 2020; Gallant & Von Damm, 2006; Humphris et al., 1995; McDermott et al., 2018). Large sulfide accumulations on the seafloor that most resemble massive sulfide ore deposits

occur in long lived (>10 ka) geothermal systems in settings lacking underlying axial magma chambers, for example the Atlantis II Deep in the slow spreading Red Sea (Bäcker & Richter, 1973), Middle Valley (Zierenberg et al., 1998), which is on an abandoned rift segment, and the TAG deposits (Humphris et al., 1995). The TAG deposit is situated in the hanging wall of a large detachment fault, which may provide a fluid pathway for fluids heated by an axial magma lens (McCaig & Harris, 2012). Large metal accumulations on the seafloor require sustained flux of high temperature hydrothermal fluids, but it is not clear that they necessarily require an actively crystallizing magmatic heat source. While the Reykjanes geothermal field could be driven by an undiscovered gabbroic intrusion at depth, there is presently no evidence that requires an active magmatic heat source.

IDDP-2 has succeeded in a long and concerted effort to drill and obtain rock samples from the high temperature reaction zone. It shows that temperatures and alteration mineral assemblages do not match the prevailing wisdom that sea floor vent fluid compositions are buffered by greenschist facies alteration of basalt and the generally unstated assumption that hydrothermal fluids are rapidly transported from the high temperature reaction zone with minimal rock alteration in the up-flow path. Studies from many geothermal fields allow clear delineation of geothermal reservoirs with significant storativity and residence times. The data presented here from the Geothermal Reservoir Transition Zone, along with previous studies from the deeper parts of the Reykjanes geothermal reservoir (Fowler et al., 2015; Marks, Schiffman, Zierenberg, Elders, et al., 2010; Marks, Schiffman, Zierenberg, Franzson, & Friðleifsson, 2010), demonstrate that greenschist facies assemblages are actively being replaced by amphibole facies assemblages. This raises the question of whether high temperature black smoker vent fluids represent conditions in the deep reaction zone or reflect continued water-rock interaction in the fluid up flow zones, as is the case with subsurface geothermal reservoirs. Unfortunately, observational constraints on the deep hydrology of active seafloor systems are essentially non-existent making direct comparison to well-studied on-land geothermal systems difficult.

Scott et al. (2017) used a coupled reactive transport model to investigate seawater recharged hydrothermal systems driven by intrusive heat sources. An important conclusion of that work is that the depth of emplacement of the heat source is a critical variable. They distinguish between shallow systems, such as that drilled by IDDP-1 in the Krafla geothermal field where high temperature interaction leads to fluid boiling, and deeper (<4 km) heat sources where phase separation occurs via brine condensation, a process often referred to as supercritical phase separation. This model was constructed prior to the deep drilling at Reykjanes but appears to be compatible with many of the observations from the IDDP-2 borehole. Phase separation by brine condensation leads to phase segregation of a halite-saturated brine and vapor-like fluid that further separate due to higher buoyancy forces of the vapor phase. Accumulation of brine and precipitation of halite in the deep reaction zone drastically changes the permeably and heat transfer in the deep reaction zone (Scott et al., 2017; Vehling et al., 2020). Rates of vapor mass flux and convective heat transfer are maximized in the brine condensation zones, in contrast to shallower systems that phase separate at lower pressures by boiling. Fluid mixing, including incorporation of recharged evolved seawater on flanks of the up-flow zone, results in temporal and spatial variations of salinity in the discharging fluid that span the full range of observed vent fluid salinities. We know that the deep fluids at Reykjanes have phase separated by condensation of a high salinity brine (Bali et al., 2020). The deepest core samples show clear evidence of rock alteration at 800°C from a vapor-like fluids, and locally, the cores record reactions with K-Fe-Cl rich brine, which results in the formation of biotite, and in one vein, K-spar.

In spite of the evidence for phase separation at 4.5 km depth, the salinity of the geothermal reservoir fluid produced at Reykjanes is very close to seawater. Does this mean that the contribution of phase-segregated seawater (brine and (or) vapor) to the production zone is minimal? Is it a reflection of incorporation of evolved recharging seawater entrained in a rising vapor plume? Is the salinity of the reservoir fluid at Reykjanes constant in time? Pope et al. (2009) propose that meteoric water recharge may have occurred when the Reykjanes peninsula was covered by glacial ice during the last Ice Age. These important questions remain to be answered. We do note that biotite, which is not expected as an alteration phase of low K basalt, has been observed in trace amount in Cores 8 and 10, where it may have formed in response to incorporation of condensed brine in the vapor-like up flow plume. Diabase from Cores 5 and 6 has a bulk composition that is as high in K_2O as the Dike 1 and 2 rocks that are in the brine condensation zone, which may reflect some brine-related alteration higher in the system.

The Reykjanes fluids also lie on a Li versus Rb plot between Endeavor Main Field fluids and sediment-hosted systems (Figure 3). Although marine sediments occur in the shallow part of the Reykjanes geothermal field, it is unlikely these trace elements are derived from marine sediment on the recharge pathway. Endeavor Main Field fluids show enrichment in ammonium and $\delta^{13}C$ depleted methane, further evidence for interaction of organic matter in sediment along the recharge path for those fluids (Butterfield et al., 1994; Lilley et al., 2003). Reykjanes fluids lack these sedimentary derived components (Óskarsson, Fridriksson, & Thorbjörnsson, 2015; Óskarsson, Inguaggiato, et al., 2015). Alternatively, the observed alkali enrichment may come from a small addition of K-Fe-Cl rich brine that is present in portions of the Pyroxene Zone to the reservoir fluid.

Phase separation in seafloor vent fluids is well established but inferring conditions in the deep high temperature reaction zone remains a challenge as fluids can both cool and react with rocks in the upflow zone. McDermott et al. (2018) have established that fluids venting at temperatures near 400°C (which is below the local boiling point) at the Piccard vent field, Mid-Cayman Rise must have phase separated at depth at temperatures at least 90° higher. Scheuermann et al. (2018) estimate subsurface temperatures at Piccard were 540°C. The Piccard fluids are depleted in chloride relative to seawater and may be a reasonable analog for the fluids responsible for the main stage Pyroxene Zone alteration in IDDP-2.

Examples of high temperature brines condensed from seawater by phase separation at high temperature are less common (Vehling et al., 2020). The highest salinity hydrothermal fluids (excluding those which have interacted with evaporites) are from the Cleft Segment of the Juan de Fuca ridge where vent fluid salinity reaches approximately twice seawater values. Wheat et al. (2020) describes results from a 32-year long time-series of sampling fluids at Vent 1 in the South Cleft Vent field. The vent temperature measured in 2016 was 338°C, which is at least 70°C lower than the minimum temperature inferred for phase separation of these high salinity brine. The temperature appears to have remained remarkably stable for more than 30 years, but the salinity of the vent has undergone a monotonic decrease from 65% higher than seawater in 1984% to 39% higher in 2016. The compositional changes are consistent with a decreasing contribution of previously phase separated brine stored in the subsurface into an active, seawater-recharged convective system. Using the composition of the phase separated brine in fluid inclusions from IDDP-2 samples (Bali et al., 2020), Wheat et al. (2020) show that the component of such brine required to be mixed into the Vent 1 fluid decreased from 5.4% in 1984% to 3.3% in 2016. Vent fluid compositions and temperatures sampled at the seafloor are a function of subsurface cooling, mixing, and rock interaction and at best represent a point in time. Inferring subsurface mineral controls on fluid composition will remain a challenging task, even if we now have direct observational evidence in the IDDP-2 borehole of the temperature, mineralogy, and mineral chemistry from the root zones of an active seawater-recharged hydrothermal system.

5. Conclusions

Fluid compositions in the seawater-recharged Reykjanes geothermal system are directly analogous to those sampled at mid-ocean ridge spreading centers after reconstructing the fluid composition to account for down hole boiling and mineral precipitation. The Reykjanes fluid compositions resemble the Endeavor Main Field, which are classified as sediment-influenced to explain slightly elevated B and alkali element concentrations, relative to basalt-hosted systems. However, Reykjanes fluids differ from the Endeavor fluids as they do not show elevated ammonium concentrations or $\delta^{13}C$ depleted methane, indications of interaction with sedimentary organic matter, suggesting the increased B and alkali elements derive from incorporation of phase-separated high salinity brine. This has been documented in fluid inclusion studies and by the presence of saline pore fluids in the deep cores from IDDP-2.

Cores recovered from sheeted dikes, which are under a hydrostatic pressure head of 4.5 km of seawater, sample the high temperature reaction zone feeding the Reykjanes geothermal system. This is a direct geochemical analog for the high temperature reaction zone postulated to occur near the sheeted dike-gabbro transition in mid-ocean ridge and ophiolite-hosted hydrothermal systems. Directional drilling at Reykjanes penetrated a well-defined, active hydrothermal up-flow chimney that feeds fluid to the Reykjanes geothermal reservoir. Evolved supercritical seawater is entering the bore hole at depths greater than 4.5 km and undergoing active phase separation producing a vapor-like fluid and a K-Fe-Cl-rich high salinity brine.

Eight independent mineral geothermometers document the temperatures of the hydrothermal alteration of the sheeted dikes, which started at temperatures well above the brittle-ductile transition for basalt and only slightly below the solidus temperature of the diabase dikes. The dikes are pervasively altered, but little changed in bulk composition, consistent with low water to rock ratio and limited fluid flux through the rocks. The main stage of alteration occurred at approximately 800°C producing the equilibrium hydrothermal mineral assemblage plagioclase-hornblende-orthopyroxene-clinopyroxene-magnetite-ilmenite-apatite-isocubanite-chalcopyrite ± quartz ± olivine ± pyrrhotite. The geothermometers define a vertical thermal gradient of 137°C/km at the time of main stage alteration. In the initial stages of alteration, a vapor-like supercritical fluid (±halite) was able to penetrate rock that had very low intrinsic permeability. Increased water activity resulted in incipient, retrograde melting. Felsic veins formed by magmatic/hydrothermal processes that ranged from crystallization of a water-rich magma-like fluid to precipitation from a silica-rich hydrothermal-like fluid. These record cooling of the system down to present-day temperatures near 600°C. Fracturing was rare in the recovered core, the upper portion of the deepest core, which is nearest to the hydrothermal feed zone, has one open fracture. The surrounding diabase exhibits hydrothermal alteration from co-existing vapor-like and K-Fe-Cl-rich hypersaline brine that condensed from supercritical altered seawater in response to pressure drop, presumably induced by fracturing in otherwise ductile rocks due to sufficiently high strain rates. The core from this upper zone contains biotite (and locally K-feldspar) in addition to the other alteration minerals that define the Pyroxene Zone alteration in the high temperature reaction zone.

The thick sequence of sheeted dikes that overly the Pyroxene Zone is altered to plagioclase and hornblende. The rocks in the Hornblende Zone show little evidence of retrograde alteration, but the Hornblende Zone alteration is actively overprinting greenschist facies alteration in the transition zone to the overlying geothermal reservoir that feeds the Reykjanes power plant. Highly productive hydrothermal feed zones that were encountered in the IDDP-2 drill hole at approximately 3,400 km depth significantly increase the potential known geothermal resource of the Reykjanes geothermal field which had previously only been explored by drilling down to approximately 2,700 m depth. In the future, it may be possible to use injection and production wells to produce 600°C fluids to drive turbines at Reykjanes, which could significantly increase power production with little change in the environmental footprint of the geothermal field. This will require considerable investment in the technology to handle 600°C fluids, including evaluation of potential corrosivity and scaling issues and the development of high-temperature well casing and casing cements.

Extensive drilling and geophysical studies conducted at Reykjanes confirm that the IDDP-2 drill hole provides a vertical transect of hydrothermal alteration in an active geothermal up-flow zone and provides the first samples of rocks undergoing active alteration by supercritical seawater in a high temperature reaction zone. Study of these samples is providing important constraints for understanding fluid-rock interaction at mid-ocean ridges, a fundamental Earth process that controls energy and chemical fluxes between the lithosphere and the hydrosphere.

Data Availability Statement

Data sets for this research and Supporting Information S1 files are archived at https://doi.org/10.5281/zenodo.5048353.

References

Acosta, M. D., Watkins, J. M., Reed, M. H., Donovan, J. J., & DePalo, D. J. (2020). Ti-in-quartz: Evaluation the role of kinetics in high temperature crystal growth experiments. *Geochimica et Cosmochimica Acta*, *281*, 149–167. https://doi.org/10.1016/j.gca.2020.04.030

Allen, R. M., Nolet, G., Morgan, W. J., Vogfjörd, K., Nettles, M., Ekström, G., et al. (2002). Plume-driven plumbing and crustal formation in Iceland. *Journal of Geophysical Research*, *107*(B8). https://doi.org/10.1029/2001jb000584

Alt, J. C., Laverne, C., Coggon, R. M., Teagle, D. A. H., Banerjee, N. R., Morgan, S., et al. (2010). Subsurface structure of a submarine hydrothermal system in ocean crust formed at the East Pacific Rise, ODP/IODP Site 1256. *Geochemistry, Geophysics, Geosystems*, *11*(10). https://doi.org/10.1029/2010GC003144

Alt, J. C., Laverne, C., Vanko, D. A., Tartarotti, P., Teagle, D. A. H., Bach, W., et al. (1996). Hydrothermal alteration of a section of upper oceanic crust in the Eastern Equatorial Pacific: A synthesis of results from Site 504 (DSDP Legs 69, 70, and 83, and ODP Legs 111, 140, and 148). *Proceedings of the Ocean Drilling Program, Scientific Results*, *148*, 417–434.

Andersen, D. J., Lindsley, D. H., & Davidson, P. M. (1993). QUILF: A PASCAL program to assess equilibria among Fe-Mg-Mn-Ti oxides, pyroxenes, olivine, and quartz. *Computers & Geosciences*, *19*, 1333–1350. https://doi.org/10.1016/0098-3004(93)90033-2

Ármannsson, H. (2016). The fluid geochemistry of Icelandic high temperature geothermal areas. *Applied Geochemistry*, *66*, 14–64. https://doi.org/10.1016/j.apgeochem.2015.10.008

Arnórsson, S. (1995). Geothermal systems in Iceland: Structure and conceptual models—I. High-temperature areas. *Geothermics*, *24*, 561–602.

Arnórsson, S., Gronvold, K., & Sigurdsson, S. (1978). Aquifer chemistry of four high temperature geothermal systems in Iceland. *Geochimica et Cosmochimica Acta*, *42*, 523–536.

Bäcker, H., & Richter, H. (1973). Die rezente hydrothermalsedimentäre lagerstätte Atlantis-II-Tiff in Roten Meer. *Geologische Rundschau*, *62*, 697–740.

Bacon, C. R., & Hirschmann, M. M. (1988). Mg/Mn partitioning as a test for equilibrium between coexisting Fe-Ti oxides. *American Mineralogist*, *7*, 57–61.

Bali, E., Aradi, L. E., Zierenberg, R. A., Diamond, L. W., Pettke, T., Szabo, Á., et al. (2020). Geothermal energy and ore-forming potential of 600°C mid-ocean-ridge hydrothermal fluids. *Geology*, *48*, 1221–1225. https://doi.org/10.1130/G47791.1

Berman, R. G., Engi, M., Greenwood, H. J., & Brown, T. H. (1986). Derivation of internally consistent thermodynamic data by the technique of mathematical programing: A review with application to the system MgO-SiO$_2$-H$_2$O. *Journal of Petrology*, *27*(6), 1331–1364. https://doi.org/10.1093/petrology/27.6.1331

Bischoff, J. L., & Rosenbauer, R. J. (1989). Liquid-vapor relations for the system NaCl-H$_2$O: Summary of the P-T-x surface from 300° to 500°C. *American Journal of Science*, *289*, 217–248. https://doi.org/10.2475/ajs.289.3.217

Blanck, H., Jousset, P., Hersir, G. P., Ágústsson, K., & Flóvenz, Ó. (2020). Analysis of 2014–2015 on- and off-shore passive seismic data on the Reykjanes Peninsula, SW Iceland. *Journal of Volcanology and Geothermal Resources*, *391*. https://doi.org/10.1016/j.jvolgeores.2019.02.001

Butterfield, D. A., McDuff, R. E., Mottl, M. J., Lilley, M. D., Lupton, J. E., & Massoth, G. J. (1994). Gradients in the composition of hydrothermal fluids from the Endeavour Segment vent field: Phase separation and brine loss. *Journal of Geophysical Research*, *99*, 9561–9583. https://doi.org/10.1029/93JB03132

Cann, J. R., McCaig, A. M., & Yardley, B. W. D. (2015). Rapid Generation of reaction permeability in the roots of black smoker systems, Troodos ophiolite, Cyprus. *Geofluids*, *15*, 179–192. https://doi.org/10.1111/gfl.12117

Cannat, M. (1993). Emplacement of mantle rocks in the seafloor at mid-ocean ridges. *Journal of Geophysical Research*, *98*, 4163–4172. https://doi.org/10.1029/92JB02221

Clague, D. A., Paduan, J. B., Caress, D. W., McClain, J., & Zierenberg, R. A. (2020). Lava flows erupted in 1996 on North Gorda Ridge segment and the geology of the nearby Sea Cliff hydrothermal vent field from 1-M resolution AUV mapping. *Frontiers in Marine Science*, *7*, 27. https://doi.org/10.3389/fmars.2020.00027

Coogan, L. (2008). Reconciling temperatures of metamorphism, fluid fluxes, and heat transport in the upper crust at intermediate to fast spreading mid-ocean ridges. *Geochemistry, Geophysics, Geosystems*, *9*(2), 19. https://doi.org/10.1029/2007gc001787

Coumou, D., Driesner, T., & Heinrich, C. (2008). The structure and dynamics of mid-ocean ridge hydrothermal systems. *Science*, *321*, 1825–1828. https://doi.org/10.1126/science.1159582

Coumou, D., Driesner, T., Weis, P., & Heinrich, C. A. (2009). Phase separation, brine formation, and salinity variation at Black Smoker hydrothermal systems. *Journal of Geophysical Research*, *114*. https://doi.org/10.1029/2008JB005764

Cowan, J., & Cann, J. (1988). Supercritical two-phase separation of hydrothermal fluids in the Troodos ophiolite. *Nature*, *333*, 259–261. https://doi.org/10.1038/333259a0

Day, H. W., Chernosky, J. V., & Kumin, H. J. (1985). Equilibria in the system MgO-SiO$_2$-H$_2$O: A thermodynamic analysis. *American Mineralogist*, *70*, 237–248.

Dick, H. J. B., Robinson, P. T., & Meyer, P. S. (1992). The plutonic foundations of a slow-spreading ridge. *American Geophysical Union Geophysical Monograph*, *70*, 1–39.

Driesner, T., & Heinrich, C. A. (2007). The system H$_2$O-NaCl. Part I. Correlation formulae for phase relations in temperature-pressure-composition space from 0 to 1000°C, 0 to 5000 bar, and 0 to 1 X$_{NaCl}$. *Geochimica et Cosmochimica Acta*, *71*, 4880–4901. https://doi.org/10.1016/j.gca.2006.01.033

Elders, W. A., Friðleifsson, G. O., Zierenberg, R. A., Pope, E. C., Mortensen, A. K., Gudmundsson, A., et al. (2011). Origin of a rhyolite that intruded a geothermal well while drilling in a basaltic volcano, at Krafla, Iceland. *Geology*, *39*, 231–234. https://doi.org/10.1130/G31393.1

Ernst, W. G., & Liu, J. (1998). Experimental phase-equilibrium study of Al- and Ti-contents of calcic amphibole in MORB—A semiquantitative thermobarometer. *American Mineralogist*, *83*, 952–969. https://doi.org/10.2138/am-1998-9-1004

Evarts, R. C., & Schiffman, P. (1983). Submarine hydrothermal metamorphism of the Del Puerto ophiolite, California. *American Journal of Science*, *283*, 289–340. https://doi.org/10.2475/ajs.283.4.289

Fowler, A. P. G. & Zierenberg, R. A. (2015). Rare earth element concentrations in geothermal fluids and epidote from the Reykjanes geothermal system, Iceland. *Proceedings World Geothermal Congress 2015, Melbourne Australia, 19–25 April 2015* (p. 10).

Fowler, A. P. G., & Zierenberg, R. A. (2016). Elemental changes and alteration recorded by basaltic drill core samples recovered from in situ temperatures up to 345°C in the active, seawater-recharged Reykjanes geothermal system, Iceland. *Geochemistry, Geophysics, Geosystems*, *17*, 4772–4801. https://doi.org/10.1002/2016gc006595

Fowler, A. P. G., Zierenberg, R. A., Reed, M., Palandri, J., Óskarsson, F., & Gunnarson, I. (2019). Rare earth element systematics in boiled fluids from basalt-hosted geothermal systems. *Geochimica et Cosmochimica Acta*, *244*, 129–154. https://doi.org/10.1016/j.gca.2018.10.001

Fowler, A. P. G., Zierenberg, R. A., Schiffman, P., Marks, N., & Friðleifsson, G. Ó. (2015). Evolution of fluid-rock interaction in the Reykjanes geothermal system, Iceland: Evidence from Iceland Deep Drilling Project core RN-17B. *Journal of Volcanology and Geothermal Research*, *302*, 47–63. https://doi.org/10.1016/j.jvolgeores.2015.06.009

Franzson, H., Thordarson, S., Bjornsson, G., Gudlaugsson, S., Richter, B., Friðleifsson, G. Ó., & Thorhallsson, S. (2002). Reykjanes high-temperature field, SW-Iceland. Geology and hydrothermal alteration of well RN-10. *27th Stanford Workshop on Geothermal Reservoir Engineering* (pp. 233–240).

Fridriksson, T., Kristjánsson, B. R., Ármannsson, H., Margrétardóttir, E., Ólafsdóttir, S., & Chiodini, G. (2006). CO$_2$ emissions and heat flow through soil, fumaroles, and steam heated mud pools at Reykjanes geothermal area, SW Iceland. *Applied Geochemistry*, *21*, 1551–1569. https://doi.org/10.1016/j.apgeochem.2006.04.006

Friðleifsson, G. Ó., Albertsson, A., Stefánsson, A., Þórólfsson, G., Mesfin, K. G., Matthíasdóttir, K. V., et al. (2020). The IDDP-2 DEEPEGS demonstrator at Reykjanes – Overview. *Proceedings World Geothermal Congress 2020, Reykjavik, Iceland* (p. 8).

Friðleifsson, G. Ó., Elders, W. A., & Albertsson, A. (2014). The concept of the Iceland deep drilling project. *Geothermics*, *49*, 2–8. Special Issue.

Friðleifsson, G. Ó., Elders, W. A., Zierenberg, R. A., Fowler, A. P. G., Weisenberger, T. B., Mesfin, K. G., et al. (2020). The Iceland Deep Drilling Project at Reykjanes: Drilling into the root zone of an analog of a black smoker. *Journal of Volcanology and Geothermal Research*, *391*. https://doi.org/10.1016/j.volgeores.2018.08.013

Friðleifsson, G. Ó., Elders, W. A., Zierenberg, R. A., Stefánsson, A., Fowler, A. P. G., Weisenberger, T. B., et al. (2017). The Iceland Deep Drilling Project 4.5 km deep well, IDDP-2, in the seawater-recharged Reykjanes geothermal field in SW Iceland has successfully reached its supercritical target. *Scientific Drilling*, *23*, 1–12.

Friðleifsson, G. Ó., Pálsson, B., Stefánsson, B., Albertsson, A., Gíslason, Þ., Gunnlaugsson, E., et al. (2020). The IDDP success story – Highlights. *Proceedings World Geothermal Congress 2020, Reykjavik, Iceland* (p. 8).

Gallant, R. M., & Von Damm, K. L. (2006). Geochemical controls on hydrothermal fluids from the Kairei and Edmond vent fields, 23°–25°S, Central Indian Ridge. *Geochemistry, Geophysics, Geosystems*, *7*(6). https://doi.org/10.1029/2005GC001067

Gee, M. A. M., Thirlwall, M. F., Taylor, R. N., Lowry, D., & Murton, B. J. (1998). Crustal processes: Major controls on Reykjanes Peninsula lava chemistry, SW Iceland. *Journal of Petrology*, *39*(5), 819–839. https://doi.org/10.1093/petroj/39.5.819

Geiger, S., Driesner, T., Heinrich, C. A., & Matthäi, S. K. (2006). Multiphase thermohaline convection in the Earth's crust: I. A new finite element – Finite volume solution technique combined with a new equation of state for NaCl-H$_2$O. *Transport in Porous Media*, *63*(3), 399–434. https://doi.org/10.1007/s11242-005-0108-z

German, C. R., & Seyfried, W. E., Jr. (2014). 8.7 Hydrothermal processes. In H. D. Holland & K. K. Turekian (Eds.), *Treatise on geochemistry* (2nd ed., pp. 191–233). Elsevier. https://doi.org/10.1016/b978-0-08-095975-7.00607-0

Ghiorso, M., & Evans, B. W. (2008). Thermodynamics of rhombohedral oxide solid solutions and a revision of the Fe-Ti two-oxide geothermometer and oxygen-barometer. *American Journal of Science*, *308*, 957–1039. https://doi.org/10.2475/09.2008.01

Gibert, B., Loggia, D., Parat, F., Escobedo, D., Levy, L., Friðleifsson, G. Ó., et al. (2020). Petrophysical properties of IDDP-2 core samples from depths of 3650 to 4650m. *Proceedings World Geothermal Congress 2020, Reykjavik, Iceland* (p. 11).

Gilgen, S. A., Diamond, L. W., & Mercolli, I. (2016). Sub-seafloor epidosite alteration: Timing, depth, and stratigraphic distribution in the Semail ophiolite, Oman. *Lithos*, *260*, 191–210. https://doi.org/10.1016/j.lithos.2016.05.014

Gillis, K. M. (2008). The roof of an axial magma chamber: A hornfelsic heat exchanger. *Geology*, *36*(4), 299–302. https://doi.org/10.1130/g24590a.1

Gillis, K. M., & Roberts, M. D. (1999). Cracking at the magma-hydrothermal transition: Evidence from the Troodos Ophiolite, Cyprus. *Earth and Planetary Science Letters*, *169*, 227–244. https://doi.org/10.1016/s0012-821x(99)00087-4

Glassley, W. E. (2010). *Geothermal energy: Renewable energy and the environment* (p. 290). CRC Press.

Hannington, M., Hardardóttir, V., Garbe-Schönberg, D., & Brown, K. L. (2016). Gold enrichment in active geothermal systems by accumulating colloidal suspensions. *Nature Geoscience*, *9*, 299–302. https://doi.org/10.1038/ngeo2661

Hardardóttir, V., Brown, K. L., Fridriksson, Þ., Hedenquist, J. W., Hannington, M. D., & Thorhallsson, S. (2009). Metal in deep liquid of the Reykjanes geothermal system, southwest Iceland: Implications for the composition of seafloor back smoker fluids. *Geology*, *37*(12), 1103–1106. https://doi.org/10.1130/G30229A.1

Hardardóttir, V., Hannington, M., Hedenquist, J., Kjarsgaard, I., & Hoal, K. (2010). Cu-rich scales in the Reykjanes geothermal system, Iceland. *Economic Geology*, *105*, 1143–1155.

Helz, R. T., & Thornber, C. R. (1987). Geothermometry of Kilauea Iki lava lake, Hawaii. *Bulletin of Volcanology*, *49*, 651–668. https://doi.org/10.1007/bf01080357

Henry, D. J., Guidotti, C. V., & Thomson, J. A. (2005). The Ti-saturation surface for low-to-medium pressure metapelitic biotites: Implications for geothermometry and Ti-substitution mechanisms. *American Mineralogist*, *90*, 316–328. https://doi.org/10.2138/am.2005.1498

Holland, T., & Blundy, J. (1994). Non-ideal interactions in calcic amphiboles and their bearing on amphibole-plagioclase thermometry. *Contributions to Mineralogy and Petrology*, *116*, 433–447. https://doi.org/10.1007/bf00310910

Hora, J. M., Kronz, A., Möller-McNett, S., & Wömer, G. (2013). An Excel-based tool for evaluating and visualizing geothermobarometry data. *Computers and Geosciences*, *56*, 178–185. https://doi.org/10.1016/j.cageo.2013.02.008

Huang, R., & Audétat, A. (2012). The titanium-in-quartz (TitaniQ) themobarometer: A critical examination and re-calibration. *Geochimica et Cosmochimica Acta*, *84*, 75–89. https://doi.org/10.1016/j.gca.2012.01.009

Humphris, S. E., Herzig, P. M., Miller, D. J., Alt, J. C., Becker, K., Brown, D., et al. (1995). The internal structure of an active sea-floor massive sulfide deposit. *Nature*, *377*, 713–716. https://doi.org/10.1038/377713a0

Humphris, S. E., & Klein, F. (2018). Progress in deciphering the controls on the geochemistry of fluids in seafloor hydrothermal systems. *Annual Reviews of Marine Science*, *10*, 315–343. https://doi.org/10.1146/annurev-marine-121916-063233

Humphris, S. E., & Thompson, G. (1978). Hydrothermal alteration of oceanic basalts by seawater. *Geochimica et Cosmochimica Acta*, *42*, 107–125. https://doi.org/10.1016/0016-7037(78)90221-1

Ingebritsen, S. E., Geiger, S., Hurwitz, S., & Driesner, T. (2010). Numerical simulation of magmatic hydrothermal systems. *Reviews of Geophysics*, *48*, 1–33. https://doi.org/10.1029/2009rg000287

Jakobsson, S. P., Jónsson, J., & Shido, F. (1978). Petrology of the Western Reykjanes Peninsula, Iceland. *Journal of Petrology*, *19*(4), 669–705. https://doi.org/10.1093/petrology/19.4.669

Jónasson, K. (2007). Silicic volcanism in Iceland: Composition and distribution within active volcanic zones. *Journal of Geodynamic*, *43*, 101–117.

Jupp, T., & Schultz, A. (2000). A thermodynamic explanation for black smoker temperatures. *Nature*, *403*, 880–883. https://doi.org/10.1038/35002552

Jupp, T., & Schultz, A. (2004). Physical balances in subseafloor hydrothermal convection cells. *Journal of Geophysical Research*, *109*, B05101. https://doi.org/10.1029/2003JB002697

Kadko, D., & Butterfield, D. A. (1998). The relationship of hydrothermal fluid composition and crustal residence time on the Juan de Fuca Ridge. *Geochimica et Cosmochimica Acta*, *62*, 1521–1533. https://doi.org/10.1016/s0016-7037(98)00088-x

Kadko, D., Gronvold, K., & Butterfield, D. (2007). Application of radium isotope to determine crustal residence times of hydrothermal fluids from two sites on the Reykjanes Peninsula, Iceland. *Geochimica et Cosmochimica Acta*, *71*, 6019–6029. https://doi.org/10.1016/j.gca.2007.09.018

Kelley, D. S., & Delaney, J. R. (1987). Two-phase separation and fracturing in mid-ocean ridge gabbros at temperatures greater than 700°C. *Earth and Planetary Science Letters*, *83*, 53–66. https://doi.org/10.1016/0012-821x(87)90050-1

Koepke, J., Berndt, J., Feig, S. T., & Holtz, F. (2007). The formation of SiO$_2$-rich melts within the deep oceanic crust by partial melting of gabbros. *Contributions to Mineralogy and Petrology*, *153*, 67–84. https://doi.org/10.1007/s00410-006-0135-y

Koepke, J., Christie, D. M., Dziony, W., Holtz, F., Lattard, D., Maclennan, J., et al. (2008). Petrography of the dike-gabbro transition at IODP Site 1256 (equatorial Pacific); The evolution of the granoblastic dikes. *Geochemistry, Geophysics, Geosystems*, *9*(7). https://doi.org/10.1029/2008gc001939

Kristmannsdóttir, H. (1979). Alteration of basaltic rocks by hydrothermal activity at 100–300°C. In M. M. Mortland & V. C. Farmer (Eds.), *International Clay Conference 1978* (pp. 359–367). Elsevier Publishing Company.

Lilley, M. D., Butterfield, D. A., Lupton, J. E., & Olson, E. J. (2003). Magmatic events can produce rapid changes in hydrothermal vent chemistry. *Nature*, *422*(6934), 878–881. https://doi.org/10.1038/nature01569

Lister, C. R. B. (1974). On the penetration of water into hot rock. *Geophysical Journal of Royal Astronomical Society*, *39*, 465–509. https://doi.org/10.1111/j.1365-246x.1974.tb05468.x

Lonker, S. W., Franzson, H., & Kristmannsdóttir, H. (1993). Mineral fluid interactions in the Reykjanes and Svartsengi geothermal systems. *American Journal of Science*, *293*, 605–670. https://doi.org/10.2475/ajs.293.7.605

Lowell, R. P., & Germanovich, L. N. (2004). Seafloor hydrothermal processes: Results from scale analysis and single-pass models. In C. R. German, J. Lin, & L. M. Parsons (Eds.), *Mid-Ocean Ridges: Hydrothermal interactions between the lithosphere and oceans* (Vol. 148, pp. 219–244). Geophysical Monographs of the American Geophysical Union.

Lundstrom, C. C. (2020). Continuously changing quartz-albite saturated melt compositions to 330°C with applications to heat flow and geochemistry of the oceanic crust. *Journal of Geophysical Research: Solid Earth*, *125*(2), e2019JB017654. https://doi.org/10.1029/2019jb017654

Marks, N., Schiffman, P., & Zierenberg, R. (2011). High-grade contact metamorphism in the Reykjanes geothermal system: Implications for fluid-rock interactions at mid-ocean ridge spreading centers. *Geochemistry, Geophysics, Geosystems*, *12*(8), 25. https://doi.org/10.1029/2011gc003569

Marks, N., Schiffman, P., Zierenberg, R., Elders, W. A., Friðleifsson, G. O., & Franzson, H. (2010). Isotopic evidence of hydrothermal exchange and seawater ingress from alteration minerals in the Reykjanes geothermal system: Results from the IDDP. *Proceedings World Geothermal Congress 2010, Bali, Indonesia* (p. 4).

Marks, N., Schiffman, P., Zierenberg, R. A., Franzson, H., & Friðleifsson, G. O. (2010). Hydrothermal alteration in the Reykjanes geothermal system: Insights from Iceland deep drilling program well RN-17. *Journal of Volcanology and Geothermal Research*, *189*, 172–190. https://doi.org/10.1016/j.jvolgeores.2009.10.018

Marsh, B. (2002). On bimodal differentiation by solidification front instability in basaltic magmas, part 1: Basic mechanics. *Geochimica et Cosmochimica Acta*, *66*(12), 2211–2229. https://doi.org/10.1016/s0016-7037(02)00905-5

Martin, E., & Sigmarsson, O. (2005). Trondhjemitic and granitic melts formed by fractional crystallization of an olivine tholeiite from Reykjanes Peninsula, Iceland. *Geological Magazine*, *142*(6), 651–658. https://doi.org/10.1017/s0016756805001160

Martins, J. E., Weemstra, C., Ruigrok, E., Verdel, A., Jousset, P., & Hersir, G. P. (2020). 3D S-wave velocity imaging of Reykjanes Peninsula high-enthalpy geothermal fields with ambient-noise tomography. *Journal of Volcanology and Geothermal Research*, *391*, 106685. https://doi.org/10.1016/j.jvolgeores.2019.106685

McCaig, A. M., & Harris, M. (2012). Hydrothermal circulation and the dike-gabbro transition in the detachment mode of slow seafloor spreading. *Geology*, *40*, 367–370. https://doi.org/10.1130/G32789.1

McDermott, J. M., Sylva, S. P., Ono, S., German, C. R., & Seewald, J. S. (2018). Geochemistry of fluids from Earth's deepest ridge-crest hot-springs: Piccard hydrothermal field, Mid-Cayman Rise. *Geochimica et Cosmochimica Acta*, *228*, 95–118. https://doi.org/10.1016/j.gca.2018.01.021

Mesfin, K. G., Sigurdsson, O., Friðleifsson, G. Ó., Zierenberg, R. A., & Weisenberger, T. B. (2020). New multisensor core (MSCL) on core from supercritical conditions. *Proceedings World Geothermal Congress 2020, Reykjavik, Iceland* (p. 5).

Ólafsson, J., & Riley, J. (1978). Geochemical studies on the thermal brine from Reykjanes (Iceland). *Chemical Geology*, *2*, 219–237.

Óskarsson, F., Fridriksson, T., & Thorbjörnsson, D. (2015). Geochemical monitoring of the Reykjanes geothermal reservoir 2003 to 2013. *Proceedings World Geothermal Congress 2015, Melbourne, Australia* (p. 9).

Óskarsson, F., Inguaggiato, S., Fridriksson, T., & Caliro, S. (2015). Gas isotope characterization of the Reykjanes geothermal field, Iceland. *Proceedings World Geothermal Congress 2015, Melbourne, Australia* (p. 6).

Paduan, J. B., Zierenberg, R. A., Clague, D. A., Spelz, R. M., Caress, D. W., Troni, G., et al. (2018). Discovery of hydrothermal fen fields on Alarcón Rise and in Southern Pescadero Basin, Gulf of California. *Geochemistry, Geophysics, Geosystems*, *19*, 4788–4819. https://doi.org/10.1029/2018gc007771

Palgan, D., Devey, C. W., & Yeo, I. A. (2020). Dike control of hydrothermal circulation in the Tertiary Icelandic crust and implications of cooling of the seafloor. *Journal of Volcanology and Geothermal Resources*, *316*, 22–33. https://doi.org/10.1016/j.jvolgeores.2016.02.021

Pichavant, M., Holtz, F., & McMillan, P. F. (1992). Phase relations and compositional dependence of H_2O solubility in quartz-feldspar melts. *Chemical Geology*, *96*, 303–319. https://doi.org/10.1016/0009-2541(92)90061-9

Pope, E., Bird, D., Arnórsson, S., Fridriksson, T., Elders, W., & Friðleifsson, G. Ó. (2009). Isotopic constraints on ice age fluids in active geothermal systems: Reykjanes, Iceland. *Geochimica et Cosmochimica Acta*, *73*(15), 4468–4488. https://doi.org/10.1016/j.gca.2009.03.033

Putirka, K. D. (2008). Thermometers and barometers for volcanic systems. *Minerals, Inclusions, and Volcanic Processes: Reviews in Mineralogy & Geochemistry*, *69*, 61–120. https://doi.org/10.1515/9781501508486-004

Reid, M., Vazquez, J. A., & Schmitt, A. K. (2011). Zircon-scale insights into the history of a Supervolcano, Bishop Tuff, Long Valley, California, with implications for the Ti-in-zircon geothermometer. *Contributions to Mineralogy and Petrology*, *161*, 293–311. https://doi.org/10.1007/s00410-010-0532-0

Richardson, C. J., Cann, J. R., Richards, H. G., & Cowan, J. G. (1987). Metal-depleted root zones of the Troodos ore-forming hydrothermal systems, Cyprus. *Earth and Planetary Science Letters*, *84*, 243–253. https://doi.org/10.1016/0012-821x(87)90089-6

Saemundsson, K., Sigurgeirsson, M. Á., & Friðleifsson, G. Ó. (2020). Geology and structure of the Reykjanes volcanic system, Iceland. *Journal of Volcanology and Geothermal Research*, *391*, 106501. https://doi.org/10.1016/j.jvolgeores.2018.11.022

Scheuermann, P. P., Tan, C., & Seyfried, W. E., Jr. (2018). Quartz solubility in the two-phase region of the $NaCl-H_2O$ system: An experimental study with applications to the Piccard hydrothermal field, Mid-Cayman Rise. *Geochemistry, Geophysics, Geosystems*, *19*, 3570–3582. https://doi.org/10.1029/2018gc007610

Schiffman, P., & Smith, B. M. (1988). Petrology and O-isotope geochemistry of a fossil seawater hydrothermal system within the Solea Graben, northern Troodos Ophiolite, Cyprus. *Journal of Geophysical Research*, *93*, 4612–4624. https://doi.org/10.1029/jb093ib05p04612

Schiffman, P., Smith, B. M., Varga, R. J., & Moores, E. M. (1987). Geometry, conditions and timing of off-axis hydrothermal metamorphism and ore deposition in the Solea Graben, N. Troodos Ophiolite, Cyprus. *Nature*, *325*, 423–425. https://doi.org/10.1038/325423a0

Schiffman, P., Zierenberg, R. A., Mortensen, A. K., Friðleifsson, G. Ó., & Elders, W. A. (2014). High temperature metamorphism in the conductive boundary layer adjacent to a rhyolite intrusion in the Krafla geothermal system, Iceland. *Geothermics*, *49*, 42–48. https://doi.org/10.1016/j.geothermics.2012.11.002

Schwarzenbach, E. M., & Steele-MacInnis, M. (2020). Fluids in submarine mid-ocean ridge hydrothermal settings. *Elements*, *16*, 389–394. https://doi.org/10.2138/gselements.16.6.389

Scott, S., Driesner, T., & Weis, P. (2017). Boiling and condensation of saline geothermal fluids above magmatic intrusions. *Geophysical Research Letters*, *44*, 1969–1705. https://doi.org/10.1002/2016GL071891

Seyfried, W. E., Jr., Berndt, M. E., & Seewald, J. S. (1988). Hydrothermal alteration processes at mid-ocean ridges: Constraints from diabase alteration experiments, hot-spring fluids and composition of the oceanic crust. *Canadian Mineralogist*, *26*, 787–825.

Seyfried, W. E., Jr., & Shanks, W. C., III. (2004). Alteration and mass transport in mid-ocean ridge hydrothermal systems: Controls on the chemical and isotopic evolution of high-temperature crustal fluids. In E. E. Davis & H. Elderfield (Eds.), *Hydrogeology of the Ocean Lithosphere* (pp. 453–496). Cambridge University Press.

Sigmundsson, F., Einarsson, P., Hjartardóttir, Á. R., Drouin, V., Jónsdóttir, K., Árnadóttir, T., et al. (2020). Geodynamics of Iceland and the signatures of plate spreading. *Journal of Volcanology and Geothermal Research*, *391*, 106436. https://doi.org/10.1016/j.jvolgeores.2018.08.014

Sigurdsson, F. (1986). Hydrogeology and groundwater on the Reykjanes Peninsula. *Jökull*, *36*, 11–29.

Spooner, E. T. C., & Fyfe, W. S. (1973). Sub-seafloor metamorphism, heat and mass transfer. *Contributions to Mineralogy and Petrology*, *42*, 187–304. https://doi.org/10.1007/bf00372607

Sun, S., & McDonough, W. F. (1989). Chemical and isotopic systematics of oceanic basalts: Implications for mantle composition and processes. In A. D. Saunders & M. J. Norry (Eds.), *Magmatism in the Ocean Basins* (Vol. *42*, pp. 313–345). Geological Society Special Publication. https://doi.org/10.1144/gsl.sp.1989.042.01.19

Tómasson, J., & Kristmannsdóttir, H. (1972). High temperature alteration minerals and thermal brines, Reykjanes, Iceland. *Contributions to Mineralogy and Petrology*, *36*, 123–134.

Vehling, F., Hasenclever, J., & Rüpke, L. (2020). Brine formation and mobilization in submarine hydrothermal systems: Insights from a novel multiphase hydrothermal flow model in the system H_2O-NaCl. *Transport in Porous Media*. https://doi.org/10.1007/s11242-020-01499-6

Violay, M., Gilbert, B., Mainprice, D., & Burg, J.-P. (2015). Brittle versus ductile deformation as the main control of the deep fluid circulation in oceanic crust. *Geophysical Research Letters*, *42*, 2767–2773. https://doi.org/10.1002/2015gl063437

Violay, M., Gibert, B., Mainprice, D., Evans, B., Dautria, J.-M., Azais, P., & Pezard, P. (2012). An experimental study of the brittle-ductile transitions of basalt at oceanic crust pressure and temperature conditions. *Journal of Geophysical Research*, *117*(B3). https://doi.org/10.1029/2011jb008884

Von Damm, K. L., & Bischoff, J. L. (1988). Chemistry of hydrothermal solutions from the Southern Juan de Fuca Ridge. *Journal of Geophysical Research*, *92*, 11334–11346.

Von Damm, K. L., Edmond, J. M., Grant, B., Measures, C. I., Walden, B., & Weiss, R. F. (1985). Submarine hydrothermal solutions at 21°N, East Pacific Rise. *Geochimica et Cosmochimica Acta*, *49*, 2197–2220. https://doi.org/10.1016/0016-7037(85)90222-4

Wanless, V. D., Perfit, M. R., Ridley, W. I., & Klein, E. (2010). Dacite petrogenesis on mid-ocean ridges: Evidence for oceanic crustal melting and assimilation. *Journal of Petrology*, *51*(12), 2377–2410. https://doi.org/10.1093/petrology/egq056

Wheat, C. G., Zierenberg, R. A., Paduan, J. B., Caress, D. W., Clague, D. A., & Chadwick, W. W., Jr. (2020). Changing brine inputs into hydrothermal fluids: Southern Cleft Segment, Juan de Fuca Ridge. *Geochemistry, Geophysics, Geosystems*, *21*(11), e2020GC009360. https://doi.org/10.1029/2020gc009360

White, R. S., McKinezie, D. P., & O'Nions, R. K. (1992). Oceanic crustal thickness from seismic measurements and rare earth element inversions. *Journal of Geophysical Research*, *97*, 19683–19715. https://doi.org/10.1029/92jb01749

Wilcock, W. S. D., & Delaney, J. R. (1996). Mid-ocean ridge sulfide deposits: Evidence for heat extraction from magma chambers or cracking fronts? *Earth and Planetary Science Letters*, *145*, 49–64. https://doi.org/10.1016/s0012-821x(96)00195-1

Zheng, Y.-F. (1993). Calculation of oxygen isotope fractionation in hydroxl-bearing silicates. *Earth and Planetary Science Letters*, *120*, 247–263. https://doi.org/10.1016/0012-821x(93)90243-3

Zierenberg, R. A., Fouquet, Y., Miller, D. J., Bahr, J. M., Baker, P. A., Bjerkgård, T., et al. (1998). The deep structure of a sea-floor hydrothermal deposit. *Nature*, *392*, 485–488. https://doi.org/10.1038/33126

Zierenberg, R. A., Fowler, A. P. G., Friðleifsson, G. Ó., Elders, W. A., & Weisenberger, T. B. (2017). Preliminary description of rocks and alteration in IDDP-2 drill core samples recovered from the Reykjanes geothermal system, Iceland. *Geothermal Resources Council Transactions*, *41*, 1599–1615.

Zierenberg, R. A., Friðleifsson, G. Ó., Elders, W. A., Schiffman, P., Fowler, A., Reed, M., et al. (2020). Active basalt alteration at supercritical conditions in IDDP-2 drill core, Reykjanes, Iceland. *Proceedings World Geothermal Congress 2020, Reykjavik, Iceland* (p. 11).

Zierenberg, R. A., Schiffman, P., Barfod, G. H., Lesher, C. E., Marks, N. E., Lowenstern, J. B., et al. (2013). Composition and origin of rhyolite melt intersected by drilling in the Krafla geothermal field. *Contributions to Mineralogy and Petrology*, *165*, 327–347. https://doi.org/10.1007/s00410-012-0811-z

References From the Supporting Information

Leake, B. E., Woolley, A. R., Arps, C. E. S., Birch, W. D., Gilbert, M. C., Grice, J. D., et al. (1997). Nomenclature of amphiboles: Report of the Subcommittee on Amphiboles of the International Mineralogical Association, Commission on New Minerals and Mineral Names. *The Canadian Mineralogist*, *35*, 219–246.

Leake, B. E., Woolley, A. R., Birch, W. D., BurkeFerraris, A. J. G., Grice, J. D., Hawthorne, F. C., et al. (2004). Nomenclature of amphiboles: Additions and revisions to the International Mineralogical Association's amphibole nomenclature. *European Journal of Mineralogy*, *16*(1), 191–196.